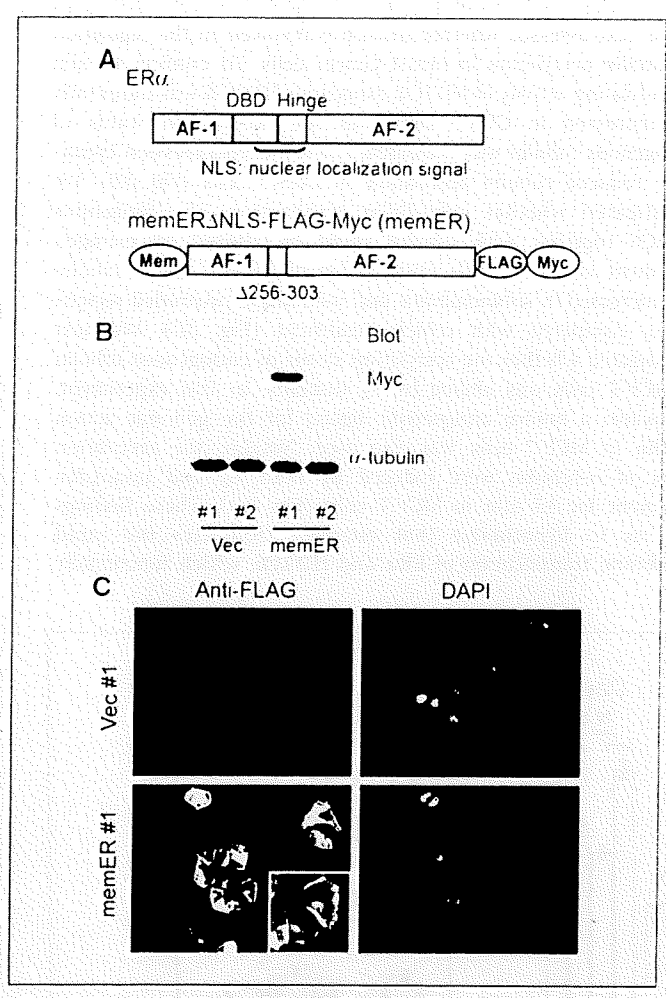

Figure 1. Generation of MCF-7 cells stably expressing memER. *A*, schematic representation of full-length ERα and memER. *B*, Western blot analysis of MCF-7 cells stably expressing memER (*memER #1* and *#2*) and vector clones (*vec #1* and *#2*). Whole cell lysates were immunoblotted with anti-Myc and anti–α-tubulin antibodies. *C*, immunocytochemistry of MCF-7 clones expressing vec #1 and memER #1. Immunostaining with anti-FLAG (*M2*) antibody shows membrane localization of ERα protein in memER #1 clone. DAPI staining shows the cell nuclei. Cells were visualized with fluorescence microscopy at a ×600 magnification. The memER #1 clone stained with anti-FLAG antibody is enlarged in the inset.

SIGMA. Alexa Fluor 488 goat anti-mouse IgG and Alexa Fluor 594 goat anti-rabbit IgG were purchased from Molecular Probe. Horseradish peroxidase–conjugated anti-mouse and anti-rabbit antibodies were purchased from Amersham Pharmacia. 17β-estradiol (E_2) and tamoxifen were purchased from SIGMA. HA-peptide was purchased from Roche.

Plasmids. Membrane-targeted ERα (memER) with FLAG and Myc epitope tags (memERΔNLS-FLAG-Myc, memER) was generated in two steps. In the first step, an expression construct of ERα with an NH_2-terminal membrane-targeting sequence (derived from the NH_2 terminus of Src kinase; MGSNKSKPKDASQ) and COOH-terminal FLAG and Myc tags was generated. In the second step, the sequence coding the nuclear localizing signal (NLS, 256-303 amino acids of ERα; ref. 10) was deleted with PCR-based sited-directed mutagenesis from the plasmid generated in the first step. The AF-1 and activation function 2 domains of ERα with the NH_2-terminal membrane-targeting sequence and COOH-terminal FLAG tag (memAF1 and memAF2, respectively) were generated as previously described (6). Deletion mutants of HDAC6 with the COOH-terminal HA tag were generated by inserting HDAC6 amplicons in pcDNA3.1(−)/Myc-His B, including the following amino acid numbers of the HDAC protein as follows: full-length HDAC6 (full), 1-1215; ΔZnF, 1-998; ΔDD2-ZnF, 1-408; ΔDD1, 409-1215; ΔDD1-DD2, 999-1215.

Cell culture and transfection. MCF-7, COS-7, and HEK293T cells were maintained in DMEM with 10% FCS at 37°C under 5% CO_2. MCF-7 and 293T cells were cultured in estrogen-starved medium (phenol red–free DMEM with 5% charcoal/dextran-treated FCS) for 2 d before E_2/tamoxifen treatment. Transfection was performed using FuGENE 6 (Roche). To establish stable transfectants, MCF-7 clones were selected using G418 (SIGMA) at a concentration of 800 μg/mL.

Immunoblotting and immunoprecipitation. Immunoblotting and immunoprecipitation were performed as previously described (6). For immunoprecipitation with the anti-HA antibody, aliquots of protein were mixed with anti-HA agarose conjugate (SIGMA).

Immunocytochemistry. Immunocytochemical analysis was performed as described (6). Nuclei were stained with 4′,6-diamidino-2-phenylindole (DAPI; SIGMA) diluted with PBS (1:10,000) for 10 min. Cells were visualized with a fluorescence microscope (KEYENCE) or Radiance 2100 confocal microscope (BIO-RAD).

Cell migration assay. The cell migration assay was performed as previously described (11). The number of MCF-7 cells migrating through a polyethylene terephthalate filter with 8-μm pores (Becton Dickinson) in 24 h was counted under microscopic examination.

Cell proliferation assay. Cells were seeded in 96-well plates at a density of 1,000 cells per well. The viable cell number was quantified using tetrazolium salt (WST-8) that could be converted to a water-soluble formazan by metabolically active cells. Spectrophotometric absorbance for formazan dye was measured at 450 nm, with absorbance at 655 nm as reference.

***In vivo* tumor growth assay.** The *in vivo* tumor growth assay was basically performed as previously described (12). Four-week-old female BALB/c nude mice were ovariectomized, and a 17β-estradiol pellet (0.72 mg; 90-d release; Innovative Research of America) was s.c. transplanted in the right shoulder of each mouse. For s.c. implantation of tumor cells, 1 million cells suspended in 100 μL of DMEM with 5% FCS were mixed with Matrigel and implanted in the left shoulder of ovariectomized nude mice. Tumor size was weekly measured at 2 to 6 wk after implantation, and tumor volume was determined using the tumor radius. Relative tumor volume was determined by normalizing to the mean value at 2 wk after implantation.

Statistical analyses. Differences between the mean values of memER-expressing MCF-7 clones and vector-expressing clones were analyzed using the Student's *t* test.

Results

Establishment of cell lines stably expressing memER. To analyze the function of membrane-localized ERα, we generated an expression vector of memER that contains the NH_2-terminal membrane-localizing sequence derived from Src kinase and lacks the NLS (Fig. 1*A*; ref. 10). Src kinase is a nonreceptor tyrosine kinase localizing at the plasma membrane with its myristoylated NH_2-terminal sequence. We established breast cancer MCF-7 cells stably expressing memER and the control vector (Fig. 1*B*). Immunocytochemical staining revealed that memER was predominantly expressed at the plasma membrane (Fig. 1*C*).

Enhanced motility and *in vivo* tumorigenesis of MCF-7 cells stably expressing memER. To elucidate the function of membrane-localized ERα, the motility of MCF-7 clones stably expressing memER and control vector was evaluated. The number of cells migrating through the 8-μm-pored polyethylene terephthalate filter in 24 h was counted. The motility of memER overexpressing MCF-7 cells (*memER #1* and *#2*) was significantly higher than that of vector clones (*vec #1* and *#2*; Fig. 2*A*). To exclude the possibility that the difference in the growth affected the cell migration, the growth rate of each clone was measured. The growth rates of memER overexpressing clones had not apparently increased

compared with control cells (Fig. 2*B*). Next, we investigated the contribution of membrane-localized ER to *in vivo* tumorigenesis by using a nude mouse xenograft model. To avoid the effect of endogenous estrogen production, nude mice were ovariectomized and estrogen pellets were inserted s.c. The results showed that tumors derived from memER clones (*memER #1* and *#2*) were larger than those from vector clones (*vec #1* and *#2*; Fig. 2*C* and *D*). Taken together, these results indicate that the overexpression of memER facilitates cell migration activity in cultured cells as well as *in vivo* tumor formation of breast cancer cells.

Rapid tubulin deacetylation as a novel nongenomic action of estrogen. We have previously revealed that tubulin could associate with the membrane-targeted AF-1 domain of ERα in MCF-7 cells (6). Tubulin is an important component of the microtubule network that regulates cell motility, which could be enhanced by HDAC6 that deacetylates tubulin (7). Thus, we investigated whether memER overexpression could modulate the acetylation status of tubulin in MCF-7 cells. Tubulin acetylation was reduced in memER-expressing clones compared with vector clones (Fig. 3*A*).

We next assessed whether HDAC6 is involved in the regulation of tubulin acetylation in breast cancer cells. To confirm tubulin deacetylating activity of HDAC6, exogenous HDAC6 was transiently overexpressed in COS-7 cells and the acetylation status of endogenous tubulin was evaluated. HDAC6 overexpression apparently reduced tubulin acetylation in COS-7 cells (Fig. 3*B*). We investigated whether subcellular localization of endogenous HDAC6 together with tubulin could be altered by estrogen treatment in MCF-7 cells. Distribution of HDAC6 and α-tubulin was increased in submembrane and membrane protruded regions by E_2 compared with vehicle treatment (Fig. 3*C*). We next investigated whether the acetylation status of endogenous tubulin in MCF-7 cells was altered by E_2 stimulus. In this experiment, tamoxifen, a known antagonistic ligand for the genomic action of ERα in MCF-7 cells, was also used. Notably, the acetylation levels of α-tubulin were reduced by both E_2 and tamoxifen treatment for 15 min in MCF-7 cells (Fig. 3*D*). These findings lead us to hypothesize that estrogen facilitates the rapid membrane translocation of ERα and HDAC6, which functionally

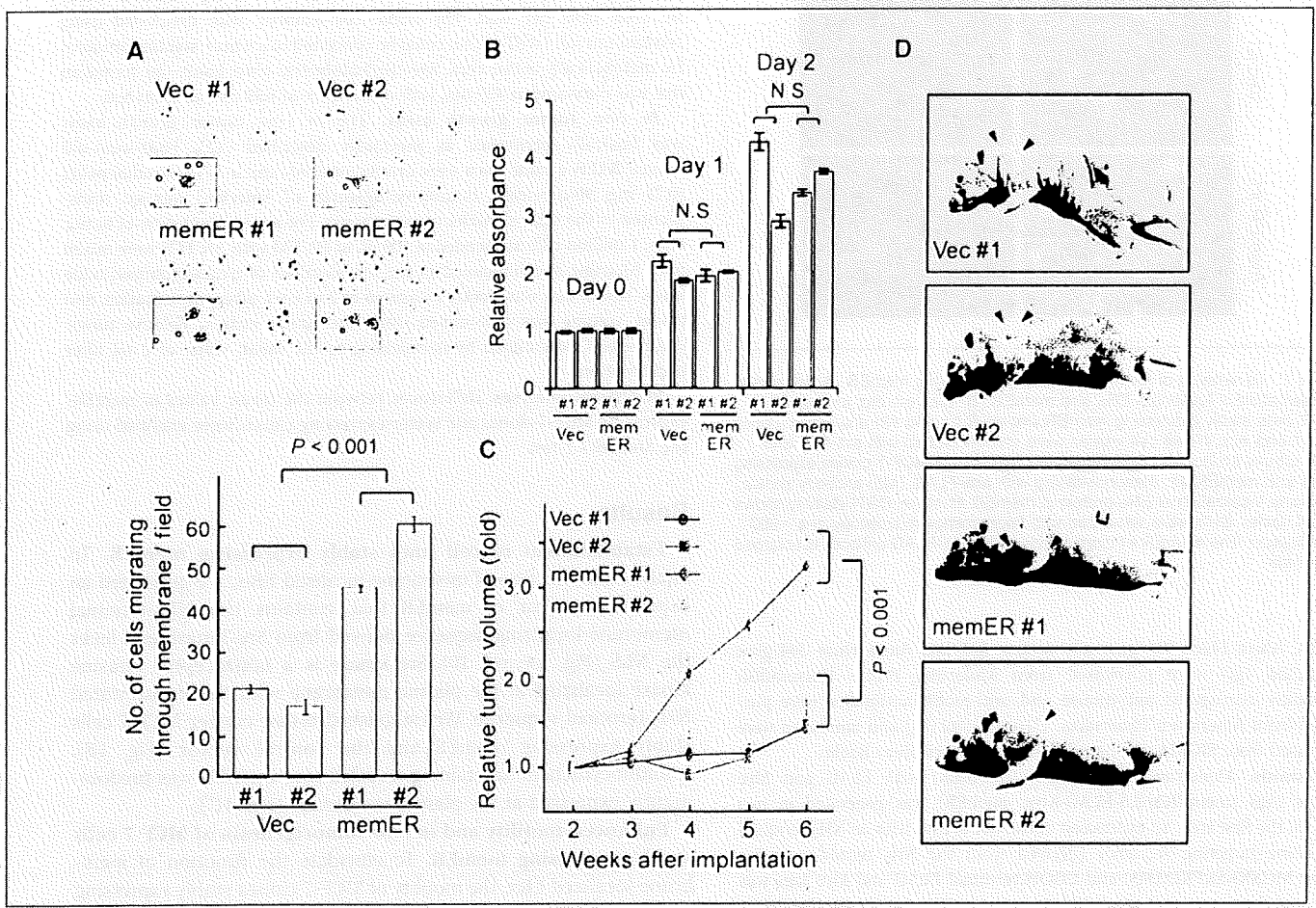

Figure 2. Enhanced motility and *in vivo* tumorigenesis of MCF-7 cells expressing memER. *A*, enhanced motility of memER-expressing MCF-7 cells. Number of cells migrating through a polyethylene terephthalate filter with 8-μm pores was counted for each clone. *Top*, cells on the lower side of the filters were stained with Giemsa's staining solution and visualized under a microscope. Representative views used to count the cells are shown at a ×200 magnification. Magnified views of membrane pores and migrating cells are shown in the insets. *Bottom, columns*, mean number of cells counted in five fields; *bars*, SE. *B*, MemER expression does not markedly affect *in vitro* cell proliferation. MCF-7 clones were seeded at a density of 1,000 cells per well and the cell growth was assayed using WST-8 tetrazolium salt. *Columns*, mean of relative absorbance at 450 nm for each clone normalized to values at day 0 ($n = 4$); *bars*, SE. *N.S.*, not significant. *C*, growth of xenograft derived from MCF-7 clones expressing memER is significantly accelerated compared with vector clones. Xenografts were established by s.c. implantation of MCF-7 clones in nude mice (one million cells per mouse). Tumor volume is shown by fold change normalized to the value at 2 wk after implantation. *Points*, mean of relative tumor volume (*vec #1*, $n = 4$; *vec #2*, $n = 3$; *memER #1*, $n = 4$; *memER #2*, $n = 7$); *bars*, SE. *D*, photographs of representative mice 8 wk after the implantation of MCF-7 clones. *Arrowhead*, tumor mass.

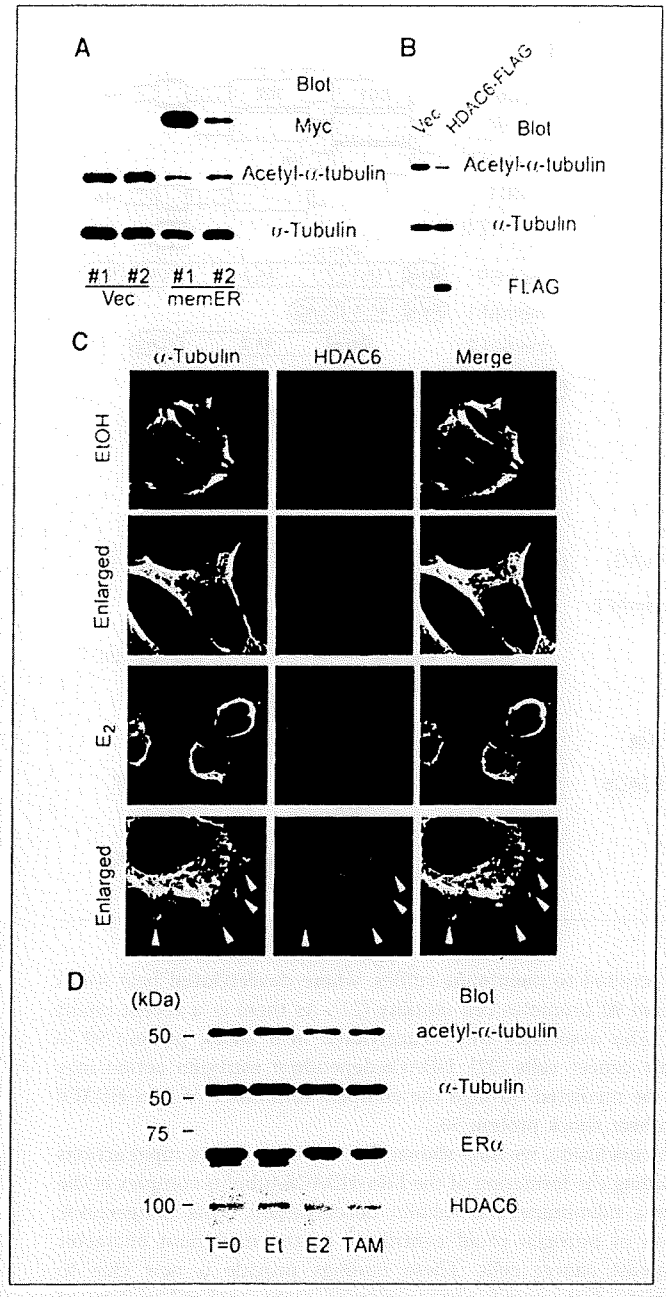

Figure 3. Estrogen reduces tubulin acetylation and translocates HDAC6 to the plasma membrane in MCF-7 cells. *A*, tubulin in memER-expressing MCF-7 clones is less acetylated. Whole cell lysates of indicated clones were immunoblotted with anti-Myc (*top*), anti–acetyl-α-tubulin (*middle*), and anti–α-tubulin (*bottom*). *B*, tubulin deacetylase activity of HDAC6. COS-7 cells were transiently transfected with empty or HDAC6-FLAG vectors. Cells were lysed at 24 h after transfection and immunoblotted with anti–acetyl-α-tubulin (*top*), anti–α-tubulin (*middle*), and anti-FLAG (M5; *bottom*). *C*, rapid translocation of HDAC6 to the plasma membrane in response to estrogen. MCF-7 cells were grown in an estrogen-starved medium for 48 h and treated with 17β-estradiol (E_2; 10 nmol/L) or vehicle (0.1% ethanol) for 15 min. Cells were immunostained with anti–α-tubulin (*green*) and anti-HDAC6 (*red*) and visualized with fluorescence microscopy at a ×600 magnification. Concentration of HDAC6 immunoreactivity at the plasma membrane is shown in E_2-stimulated cells. *Enlarged panels*, magnified views of a part of the top panels. Membrane protrusions (*white arrowheads*) are shown in enlarged panels of E_2-stimulated cells. *D*, rapid deacetylation of tubulin in MCF-7 cells with estrogen stimulation. MCF-7 cells were treated with E_2 (100 nmol/L), tamoxifen (*TAM*; 10 μmol/L), or vehicle (*Et*) for 15 min. Whole-cell lysates before (*T = 0*) and after drug treatment were immunoblotted with anti–acetyl-α-tubulin (*top*), anti–α-tubulin (*top middle*), anti-ERα (*bottom middle*), and HDAC6 (*bottom*). The acetylated level of tubulin is reduced in lysates from E_2- and tamoxifen-stimulated cells.

interact with the microtubule network and cause tubulin deacetylation.

Ligand-dependent association of HDAC6 with ERα. To prove the hypothesis that ERα associates with HDAC6 at the plasma membrane, memER and HA-tagged HDAC6 were cotransfected in 293T cells. An immunoprecipitation study verified the physical interaction of memER and HDAC6 proteins in an E_2-dependent manner. Tamoxifen also induced a weak interaction between memER and HDAC6 (Fig. 4*A*).

To analyze the responsible domains for the association of HDAC6 and memER, we generated a series of HA-tagged HDAC6 expression vectors with various functional domains deleted (Fig. 4*B*). HDAC6 includes two deacetylase domains (DD1 and DD2) and one ubiquitin carboxyl-terminal hydrolase-like zinc finger domain (ZnF-UBP). A transfection study revealed that these HDAC6 deletion mutants were expressed predominantly in the cytoplasm (data not shown). As ERα deletion mutants, we used memAF1 and memAF2 expression vectors, including the entire A/B region of ERα containing the AF-1 domain and the entire E/F region containing the activation function 2 domain, respectively, with an NH_2-terminal membrane-targeted sequence. We previously showed that these ERα deletion mutants were predominantly localized in the cytoplasm (6). The immunoprecipitation study revealed that the membrane-targeted activation function 2 domain associated with HDAC6 (Fig. 4*C*), and the DD2 domain of HDAC6 was responsible for the interaction with memER (Fig. 4*D*).

Discussion

Posttranslational modification is an important factor for the regulation of protein structure and function. Phosphorylation by protein kinases such as phosphatidylinositol-3-OH kinase and mitogen-activated protein kinase has been shown to play a critical role in estrogen-dependent nongenomic action. In the present study, we show that estrogen caused the formation of the ERα-HDAC6-tubulin complex at the plasma membrane and rapid tubulin deacetylation in MCF-7 breast cancer cells. Our findings show a novel aspect of estrogen nongenomic action that is regulated by tubulin acetylation, which is distinct from the previously reported mechanism dependent on protein phosphorylation.

In MCF-7 cells, estrogen-dependent tubulin deacetylation would be one of the driving forces of cell motility, as the microtubule network including tubulin is a critical element in cell migration. Our findings are consistent with a previous report that HDAC6 overexpression caused tubulin deacetylation and enhanced motility of breast cancer cells and the inhibition of HDAC6 activity reduced motility (9). HDAC6 inhibition is also considered to decrease turnover of focal adhesion, an interface between the cell membrane and the extracellular matrix. Decreased turnover of focal adhesion results in reduced cell motility (13).

It is also notable that memER accelerated tumor growth of MCF-7 cells in nude mice without enhancing cell proliferation *in vitro*. *In vivo* tumor growth differs from *in vitro* proliferation in the aspect that *in vivo* tumor growth requires several factors including anoikis resistance, angiogenesis, and survival in the hypoxic environment. Anoikis is a form of apoptosis caused by absence of attachment to the extracellular matrix (14). It was reported recently that HDAC6 is critical for anoikis resistance and *in vivo* tumorigenic growth with human ovarian cancer SKOV3 cells (15). In another report, stability of microtubules was shown to be associated with anoikis through alteration of the focal adhesion

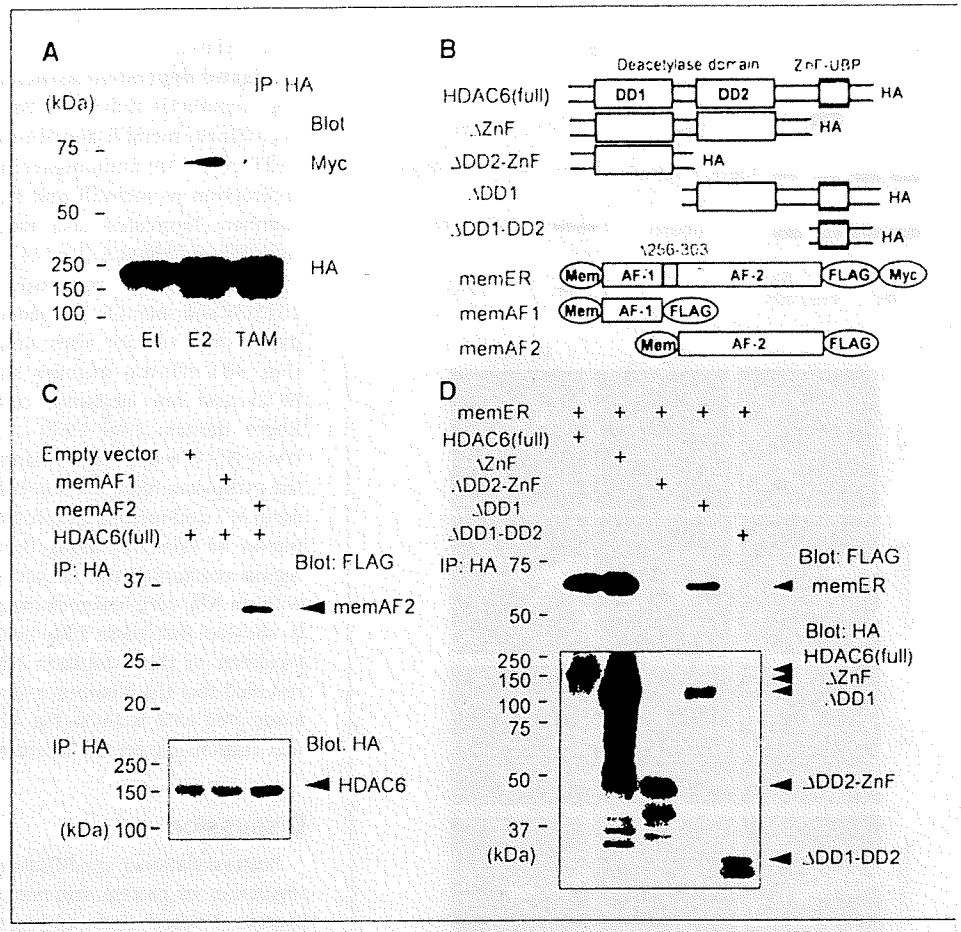

Figure 4. MemER associates with HDAC6. *A*, ligand-dependent association of memER and HDAC6. 293T cells were grown in estrogen-starved medium for 24 h and cotransfected with memER and HDAC6-FLAG. After 24-h incubation, cells were treated with E_2 (100 nmol/L), tamoxifen (10 μmol/L), and vehicle for 6 h. Whole cell lysates were immunoprecipitated with anti-HA. Immunoprecipitants by anti-Myc were subjected to immunoblotting with anti-Myc antibody (*top*) and anti-HA antibody (*bottom*). *B*, schematic representation of deletion mutants of HA-tagged HDAC6 and memER. *C*, ERα binds to HDAC6 through its activation function 2 domain. 293T cells were cotransfected with HDAC6-HA (full) and FLAG-tagged ERα deletion mutants. After 24-h incubation, cells were lysed and immunoprecipitated with anti-HA. Immunoprecipitants were immunoblotted with anti-FLAG (M5) antibody (*top*) and anti-HA antibody (*bottom*). *D*, HDAC6 binds to ERα with its deacetylase domain 2. 293T cells were cotransfected with memER and HA-tagged HDAC6 plasmids. After 24-h incubation, cells were lysed and immunoprecipitated with anti-HA. Immunoprecipitants were immunoblotted with anti-FLAG (M5) antibody (*top*) and anti-HA antibody (*bottom*).

structure (16). Although the direct effect of tubulin deacetylation is not evaluated in these reports, it is possible that deacetylated tubulin affects focal adhesion turnover and regulates anoikis resistance.

Because HDAC6 itself is reported as an estrogen-induced gene and HDAC6 overexpression is shown to enhance cell motility (8, 9), the estrogen-dependent up-regulation of HDAC6 could further potentiate its enzymatic activity. In this case, the genomic action of estrogen would promote its nongenomic action in MCF-7 cells. In contrast, the tamoxifen-induced nongenomic action would be unfavorable for the antagonistic function of this drug in the genomic action. We showed that tamoxifen also caused the interaction of memER with HDAC6 and tubulin deacetylation in MCF-7 cells. We assume that HDAC6-dependent tubulin deacetylation contributes to the increased cell motility and invasive migration of breast cancer cells; thus, this nongenomic action of the tamoxifen-induced tubulin deacetylation could be one of the reasons for tamoxifen resistance in breast cancer treatment. Indeed, several clinical trials have shown the superiority of aromatase inhibitors over tamoxifen in the first-line endocrine therapy for postmenopausal women with both early-stage and advanced breast cancers (17, 18). There is also a report that has shown tamoxifen-induced redistribution of ERα to the extranuclear region and the activation of nongenomic action via the epidermal growth factor receptor pathway (19), which would provide another mechanism for tamoxifen resistance.

HDAC6 also deacetylates another cytosolic protein, heat shock protein 90 (20). It has been shown that heat shock protein 90 could be recruited to membrane ruffles, where deacetylated heat shock protein 90 promotes cell motility (21). As there is a recent report that ERα associates with deacetylated heat shock protein 90 in breast cancer cells (22), HDAC6-dependent estrogen action may also be mediated through the complex formation of ERα-HDAC6 with heat shock protein 90.

In conclusion, we have shown that estrogen exerts rapid actions including the formation of the ERα-HDAC6-tubulin complex at the plasma membrane and tubulin deacetylation. This nongenomic action of estrogen could contribute to the malignant character of breast cancer cells. These findings provide a new clue to understand the mechanisms underlying the pathophysiology of breast cancer and the resistance to endocrine therapy, and to develop new molecular targets for breast cancer treatment.

Disclosure of Potential Conflicts of Interest

No potential conflicts of interest were disclosed.

Acknowledgments

Received 9/9/08; revised 1/6/09; accepted 1/9/09; published OnlineFirst 3/24/09.

Grant support: Genome Network Project and DECODE from the Ministry of Education, Culture, Sports, Science and Technology; Grants from the Japan Society for the Promotion of Science, and Grants-in-Aid from the Ministry of Health, Labor and Welfare.

The costs of publication of this article were defrayed in part by the payment of page charges. This article must therefore be hereby marked *advertisement* in accordance with 18 U.S.C. Section 1734 solely to indicate this fact.

We thank Dr. Stuart L. Schreiber for providing HDAC6 cDNA and A. Okada for his technical assistance.

References

1. Rabaglio M, Aebi S, Castiglione-Gertsch M. Controversies of adjuvant endocrine treatment for breast cancer and recommendations of the 2007 St Gallen conference. Lancet Oncol 2007;8:940–9.
2. Cheskis BJ, Greger JG, Nagpal S, Freedman LP. Signaling by estrogens. J Cell Physiol 2007;213:610–7.
3. Simoncini T, Hafezi-Moghadam A, Brazil DP, et al. Interaction of oestrogen receptor with the regulatory subunit of phosphatidylinositol-3-OH kinase. Nature 2000;407:538–41.
4. Kousteni S, Bellido T, Plotkin LI, et al. Nongenotropic, sex-nonspecific signaling through the estrogen or androgen receptors: dissociation from transcriptional activity. Cell 2001;104:719–30.
5. Migliaccio A, Di Domenico M, Castoria G, et al. Tyrosine kinase/p21ras/MAP-kinase pathway activation by estradiol-receptor complex in MCF-7 cells. EMBO J 1996;15:1292–300.
6. Azuma K, Horie K, Inoue S, Ouchi Y, Sakai R. Analysis of estrogen receptor α signaling complex at the plasma membrane. FEBS Lett 2004;577:339–44.
7. Hubbert C, Guardiola A, Shao R, et al. HDAC6 is a microtubule-associated deacetylase. Nature 2002;417:455–8.
8. Yoshida N, Omoto Y, Inoue A, et al. Prediction of prognosis of estrogen receptor-positive breast cancer with combination of selected estrogen-regulated genes. Cancer Sci 2004;95:496–502.
9. Saji S, Kawakami M, Hayashi S, et al. Significance of HDAC6 regulation via estrogen signaling for cell motility and prognosis in estrogen receptor-positive breast cancer. Oncogene 2005;24:4531–9.
10. Rai D, Frolova A, Frasor J, Carpenter AE, Katzenellenbogen BS. Distinctive actions of membrane-targeted versus nuclear localized estrogen receptors in breast cancer cells. Mol Endocrinol 2005;19:1606–17.
11. Azuma K, Tanaka M, Uekita T, et al. Tyrosine phosphorylation of paxillin affects the metastatic potential of human osteosarcoma. Oncogene 2005;24:4751–64.
12. Urano T, Saito T, Tsukui T, et al. Efp targets 14-3-3 σ for proteolysis and promotes breast tumour growth. Nature 2002;417:871–5.
13. Tran AD, Marmo TP, Salam AA, et al. HDAC6 deacetylation of tubulin modulates dynamics of cellular adhesions. J Cell Sci 2007;120:1469–79.
14. Reddig PJ, Juliano RL. Clinging to life: cell to matrix adhesion and cell survival. Cancer Metastasis Rev 2005;24:425–39.
15. Lee YS, Lim KH, Guo X, et al. The cytoplasmic deacetylase HDAC6 is required for efficient oncogenic tumorigenesis. Cancer Res 2008;68:7561–9.
16. Deschesnes RG, Patenaude A, Rousseau JL, et al. Microtubule-destabilizing agents induce focal adhesion structure disorganization and anoikis in cancer cells. J Pharmacol Exp Ther 2007;320:853–64.
17. Thurlimann B, Keshaviah A, Coates AS, et al. A comparison of letrozole and tamoxifen in postmenopausal women with early breast cancer. N Engl J Med 2005;353:2747–57.
18. Mouridsen H, Gershanovich M, Sun Y, et al. Phase III study of letrozole versus tamoxifen as first-line therapy of advanced breast cancer in postmenopausal women: analysis of survival and update of efficacy from the International Letrozole Breast Cancer Group. J Clin Oncol 2003;21:2101–9.
19. Fan P, Wang J, Santen RJ, Yue W. Long-term treatment with tamoxifen facilitates translocation of estrogen receptor α out of the nucleus and enhances its interaction with EGFR in MCF-7 breast cancer cells. Cancer Res 2007;67:1352–60.
20. Kovacs JJ, Murphy PJ, Gaillard S, et al. HDAC6 regulates Hsp90 acetylation and chaperone-dependent activation of glucocorticoid receptor. Mol Cell 2005;18:601–7.
21. Gao YS, Hubbert CC, Lu J, et al. Histone deacetylase 6 regulates growth factor-induced actin remodeling and endocytosis. Mol Cell Biol 2007;27:8637–47.
22. Fiskus W, Ren Y, Mohapatra A, et al. Hydroxamic acid analogue histone deacetylase inhibitors attenuate estrogen receptor-α levels and transcriptional activity: a result of hyperacetylation and inhibition of chaperone function of heat shock protein 90. Clin Cancer Res 2007;13:4882–90.

Expression of CUB domain containing protein (CDCP1) is correlated with prognosis and survival of patients with adenocarcinoma of lung

Jun-ichiro Ikeda,[1] Tomofumi Oda,[1,2] Masayoshi Inoue,[2] Takamasa Uekita,[3] Ryuichi Sakai,[3] Meinoshin Okumura,[2] Katsuyuki Aozasa[1] and Eiichi Morii[1,4]

Departments of [1]Pathology and [2]Thoracic Surgery, Osaka University Graduate School of Medicine, 2-2 Yamada-oka, Suita, Osaka, and [3]Growth Factor Division, National Cancer Center Research Institute, 5-1-1 Tsukiji, Chuo-ku, Tokyo, Japan

(Received September 29, 2008/Revised November 4, 2008/Accepted November 19, 2008/Online publication December 11, 2008)

CUB domain containing protein (CDCP1), a transmembrane protein with intracellular tyrosine residues which are phosphorylated upon activation, is supposed to be engaged in proliferative activities and resistance to apoptosis of cancer cells. Expression level of CDCP1 was examined in lung adenocarcinoma, and its clinical implications were evaluated. CDCP1 expression was immunohistochemically examined in lung adenocarcinoma from 200 patients. Staining intensity of cancer cells was categorized as low and high in cases with tumor cells showing no or weak and strong membrane staining, respectively. MIB-1 labeling index was also examined. There were 113 males and 87 females with median age of 63 years. Stage of disease was stage I in 144 cases (72.0%), II in 19 (9.5%), and III in 37 (18.5%). Sixty of 200 cases (30.0%) were categorized as CDCP1-high, and the remaining as CDCP1-low. Significant positive correlation was observed between CDCP1-high expression and relapse rate ($P < 0.0001$), poor prognosis ($P < 0.0001$), MIB-1 labeling index ($P < 0.0001$), and occurrence of lymph node metastasis ($P = 0.0086$). There was a statistically significant difference in disease-free survival (DFS) ($P < 0.0001$) and overall survival (OS) rates ($P < 0.0001$) between patients with CDCP1-high and CDCP1-low tumors. Univariate analysis showed that lymph node status, tumor stage, and CDCP1 expression were significant factors for both OS and DFS. Multivariate analysis revealed that only CDCP1 expression was an independent prognostic factor for both OS and DFS. CDCP1 expression level is a useful marker for prediction of patients with lung adenocarcinoma (*Cancer Sci* 2009; 100: 429–433).

Introduction

Since 1985 lung cancer has been the most common cause of cancer death in the world.[1] Non-small cell lung cancer (NSCLC) comprises 75–85% of all lung cancers, and approximately two-thirds of NSCLC patients have advanced stages at diagnosis. Despite the advances in the methods for detection and treatment of lung cancer, prognosis of NSCLC patients still remains unfavorable. Therefore, it is important to clarify the mechanism of tumor biology, and establishment of effective therapeutic modalities is essential to improve the prognosis in NSCLC. Previous studies accumulated information regarding the factors influencing prognosis in NSCLC. They include clinical, pathological, and molecular factors.

CUB domain containing protein (CDCP1) was originally identified as an epithelial tumor antigen by comparisons of molecules expressed in lung cancer cell lines and normal lung tissues.[2] CDCP1 is a transmembrane protein with three extracellular CUB domains, which are important for cell–cell interactions, and intracellular tyrosine residues which are phosphorylated upon activation.[2–7] Previously, we reported the epigenetic regulation of CDCP1 expression in the cell lines derived from various malignancies and clinical samples of breast cancer.[8,9] The CDCP1 expression level correlated with proliferative activities of breast cancer cells in the clinical samples.[8] Very recently, CDCP1 was reported to protect cells from anoikis, a form of apoptosis triggered by the loss of cell survival signals generated from interaction of cells with the extracellular matrix.[10] The knocked-down expression of CDCP1 by RNA interference abolished in vitro colony formation and in vivo metastatic abilities of lung adenocarcinoma cell line A549.[10] These findings showed that CDCP1 is required for protection of cells from anoikis, and suggest an important role of CDCP1 for tumorigenesis and metastasis, at least in cell lines. In the present study, CDCP1 expression was immunohistochemically examined in clinical samples from lung adenocarcinoma, and its clinical implications were evaluated.

Materials and Methods

Patients and tissue samples. Two hundred patients who underwent surgery for lung adenocarcinoma at Osaka University Hospital during the period from January 1993 to January 2004 were examined. Clinicopathological findings in these 200 patients are summarized in Table 1. There were 113 men and 87 women with ages ranging from 33 to 82 years (median, 63). Resected specimens were macroscopically examined to determine the location and size of the tumors. The size of the main tumor ranged from 8 to 70 mm (median, 24.5). The histological stage was determined according to the 6th edition of the Union International Contre le Cancer – TNM staging system.[11] Histologic specimens were fixed in 10% formalin and routinely processed for paraffin-embedding. Paraffin-embedded specimens were stored in the dark room in the Department of Pathology of Osaka University Hospital at room temperature, and were sectioned at 4-μm thickness at the time of staining. In some cases, total RNA was extracted using RNeasy kit (Qiagen, Valencia, CA, USA) with DNase I treatment. All patients were followed up with laboratory examinations including routine peripheral blood cell counts at 1- to 6-month intervals, chest roentgenogram, computed tomographic scan of the chest, and endoscopic examinations of the bronchus at 6- to 12-month intervals. The follow-up period for survivors ranged from 5 to154 months (median, 63). The study was approved by the ethical review board of the Graduate

This work is original, and contains no materials previously presented in any reports and publications.

[4]To whom correspondence should be addressed.
E-mail: morii@patho.med.osaka-u.ac.jp

doi: 10.1111/j.1349-7006.2008.01066.x

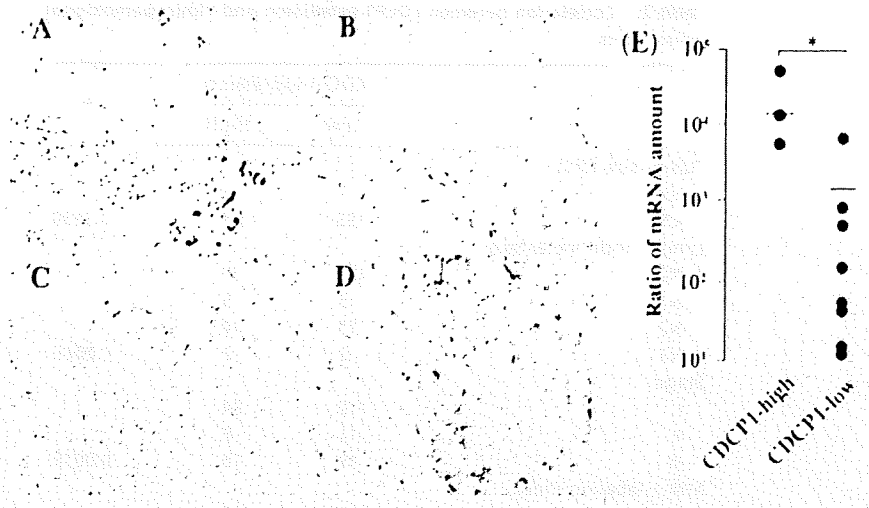

Fig. 1. Surface staining of CDCP1-low (A and B) and -high (C and D) cases, ×400 (E) Real-time reverse transcription–polymerase chain reaction. The amount of CDCP1 mRNA was significantly higher in immunohistochemically defined CDCP1-high cases than in CDCP1-low cases. The bar shows mean values of the amount of CDCP1 mRNA. *$P < 0.01$

Table 1. Summary of characteristics in 200 pulmonary adenocarcinoma patients

Sex	Number of patients
Male	113
Female	87
Tumor size (cm)	
≥5	12
<5	187
Lymph node metastasis	
N0	159
N1	8
N2	29
N3	4
Stage	
I	144
II	19
III	37
Recurrence	
Positive	60
Negative	140
Prognosis	
Dead	41
Alive (with recurrence)	24
Alive (with no recurrence)	135

School of Medicine, Osaka University. Informed consent was obtained from each patient.

Immunohistochemistry for CDCP1, phosphorylated CDCP1 and Ki-67. CDCP1 expression was immunohistochemically examined with use of anti-CDCP1 (Abcam Ltd, Cambridge, UK) and antiphosphorylated CDCP1 antibody. The antiphosphorylated CDCP1 antibody recognizes CDCP1 phosphorylated at Tyr734 and can be used for immunostaining on paraffin-embedded sections.[10,12] The proliferative activity of cancer cells was examined with monoclonal antibody MIB-1 (Immunotech, Marseilles, France), recognizing the proliferation-associated antigen Ki-67. After antigen retrieval with Pascal pressurized heating chamber (Dako, Glostrup, Denmark), the sections were incubated with anti-CDCP1, phosphorylated CDCP1 antibody and MIB-1, diluted at ×200, ×400 and ×100, respectively. Then, the sections were treated with biotin-conjugated antigoat IgG (Zymed, San Francisco, CA, USA) for CDCP1 staining, or with biotin-conjugated antimouse IgG (Dako) for phosphorylated CDCP1 and MIB-1 staining. After washing, the sections were incubated with the peroxidase-conjugated biotin-avidin complex (Vectastain ABC kit, Vector Laboratories, Burlingame, CA, USA). diaminobenzidine (Vector Laboratories) was used as a chromogen. As the negative control, staining was carried out in the absence of a primary antibody. Stained sections were evaluated independently by two pathologists (JI and EM). Generally, CDCP1 expression levels varied among tumor cells in the same case. Staining intensity of tumor cells was divided into four categories: tumor cells with no (representative field was demonstrated in Fig. 1A), weak (Fig. 1B), moderate (Fig. 1C), or strong (Fig. 1D) membrane staining. The intensity of CDCP1 expression in each case was defined by the major population of staining as follows: cases with tumor cells showing no or weak membrane staining were categorized as CDCP1-low, and those showing moderate or strong membrane staining as CDCP1-high. The MIB-1 labeling index was defined as the percentage of stained nuclei per 1000 cells. The cases were divided into MIB-1-high and MIB-1-low groups using the median as cut-off value.

Quantification of mRNA by real-time reverse transcription-polymerase chain reaction (RT-PCR). To evaluate the specificity of CDCP1 immunostaining, expression level of CDCP1 at mRNA and protein levels was compared. For this, fresh frozen materials were available in 13 of the 200 cases. Total RNA was extracted using RNeasy kit (Qiagen, Valencia, CA, USA) with DNase I treatment. Two micrograms of total RNA was subjected to reverse transcription using Superscript III (Invitrogen, Carlsbad, CA, USA). The mRNA levels for CDCP1 and glyceraldehyde-3-phosphate dehydrogenase (GAPDH) genes were verified using TaqMan Gene Expression Assays (Hs00224587_m1 and 4310884E, respectively; Applied Biosystems, Foster City, CA, USA) as recommended by the manufacturer. The amount of CDCP1 mRNA was normalized to that of GAPDH mRNA.

Statistical analysis. Statistical analyses were performed using StatView software (SAS Institute Inc., Cary, NC, USA). The Chi-square and Fisher's exact probability test were used to analyze the correlation between CDCP1 expression and clinicopathological factors in pulmonary adenocarcinoma. Kaplan-Meier methods were used to calculate overall survival (OS) and disease-free survival (DFS) rate, and differences in survival curves were evaluated with the log-rank test. Cox's proportional hazards regression model with a stepwise manner was used to analyze the independent prognostic factors. The P-values of less than 0.05 were considered to be statistically significant.

Results

Tumor stages in the present patients were: stage I in 144 patients (72.0%); II in 19 patients (9.5%); and III in 37 patients (18.5%). The histological types of tumors were: bronchioloalveolar

doi: 10.1111/j.1349-7006.2008.01066.x

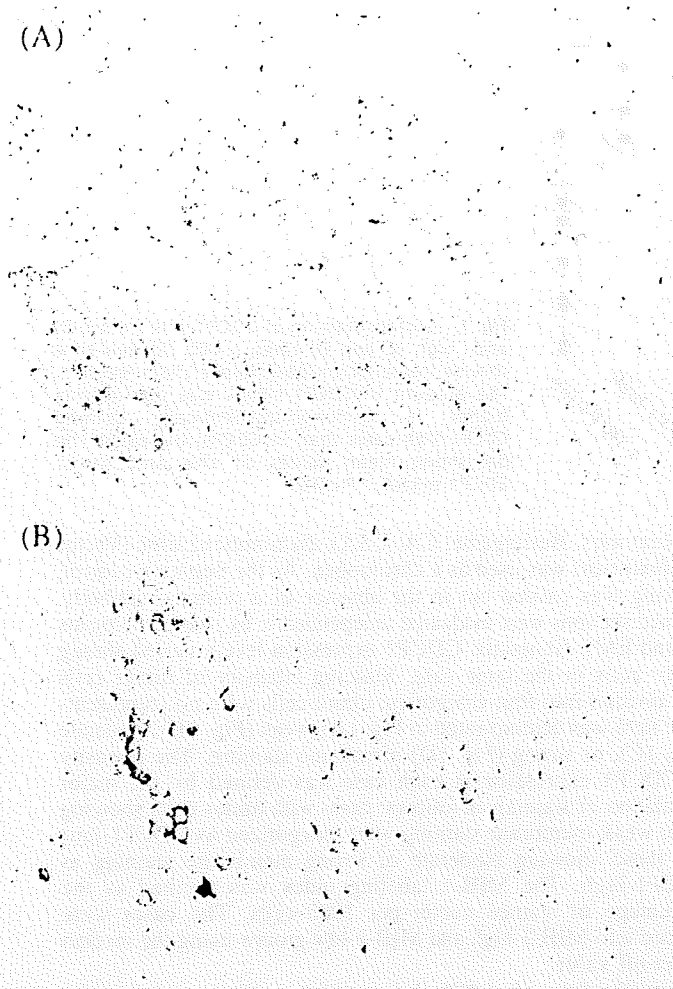

Fig. 2. Localization of phosphorylated CDCP1 in lung adenocarcinoma. Stained cells with anti-CDCP1 antibody (A), and antiphosphorylated CDCP1 antibody (B). Among the CDCP1-positive tumor cells, peripheral areas of tumor cell nests were stained with antiphophorylated CDCP1 antibody, ×400.

(62 patients, 31.0%); papillary (48 patients, 24.0%); or mixed bronchioloalveolar and papillary adenocarcinoma (90 patients, 45.0%). The 5-year DFS and OS was 78.7% and 80.6%, respectively. Tumors recurred in 60 patients. Of these, 38 patients died due to the tumors.

To evaluate the specificity of immunohistochemical staining for CDCP1 expression, quantitative real-time RT-PCR was performed: expression levels of CDCP1 at protein and mRNA level was compared in 13 cases (3 CDCP1-high and 10 CDCP1-low cases at immnohistochemical results). The amount of CDCP1 mRNA was significantly higher in cases with CDCP1-high expression at immunohistochemistry than those with CDCP1-low expression ($P < 0.01$, Fig. 1E). These results showed that the immunohistochemical evaluation is a reliable method for evaluation of CDCP1 expression.

Immunohistochemical detection of CDCP1 expression was carried out in 200 lung adenocarcinoma tissues. Sixty of 200 cases (30.0%) were categorized as CDCP1-high, and the remaining as CDCP1-low. Representative staining results were illustrated in Fig. 1(A–D).

Intracellular tyrosine residues of CDCP1 are known to be phosphorylated upon activation in vitro. To examine the localization of activated CDCP1, 43 cases of CDCP1-high lung adenocarcinoma tissues were stained with antiphosphorylated CDCP1. Phosphorylated CDCP1 was detected only in a small portion of CDCP1-expressing cells (Fig. 2 A and 2B), which

Table 2. Correlation between CDCP1 expression and clinicopathological parameters

	CDCP1 expression		*P*
	Low	High	
Tumor size (cm)			
≥5	7	5	
<5	133	55	0.3630
Lymph node metastasis			
N0	120	39	
N1	3	5	
N2	15	14	
N3	2	2	0.0086
Stage			
I	110	34	
II	11	8	
III	19	18	0.0059
MIB-1 labeling index			
≥5%	56	45	
<5%	84	15	<0.0001
Recurrence			
Positive	23	37	
Negative	117	23	<0.0001
Prognosis			
Dead	17	24	
Alive (with recurrence)	10	14	
Alive (with no recurrence)	113	22	<0.0001

appeared to be localized to the peripheral areas of tumor cell nests. Cells without CDCP1 expression did not show any phosphorylated CDCP1 signals, indicating the specificity of the antiphophorylated CDCP1 antibody. Phosphorylated CDCP1 was detected in 19 out of 43 cases: any significant clinicopathological differences were not observed between cases with and without phosphorylated CDCP1.

Correlation of CDCP1 expression with the clinicopathological features was evaluated. Significant positive correlation was observed between CDCP1-high expression and relapse rate ($P < 0.0001$), poor prognosis ($P < 0.0001$), MIB-1 labeling index ($P < 0.0001$), and occurrence of lymph node metastasis ($P = 0.0086$). Other parameters including tumor size and stage did not correlate with CDCP1 expression (Table 2). There was a statistically significant difference in DFS rates ($P < 0.0001$) and OS rates ($P < 0.0001$) between patients with CDCP1-high and CDCP1-low tumors (Fig. 3).

Univariate analysis showed that lymph node status, tumor stage, and CDCP1 expression were significant factors for both OS and DFS (Table 3). The multivariate analysis revealed that only CDCP1 expression was an independent prognostic factor for both OS and DFS.

Discussion

Patient characteristics such as the gender (male preponderance), age distribution (median age, 6th decades of life), and 5-year OS of approximately 80% in the present study were similar to those in a previous report on the lung adenocarcinoma.[13] In addition, the univariate analysis showed the prognostic significance of occurrence of lymph node metastasis and stage of disease, as reported previously.[13] These findings indicate that the results obtained from the present cases are commonly applicable.

Among the clinicopathological factors examined, high CDCP1 expression level correlated with increased occurrence of lymph node metastasis and tumor relapse. A previous study using the lung adenocarcinoma cell lines indicated a significant role of CDCP1 for anchorage-independent growth of tumor cells.[10]

Table 3. Univariate and multivariate analyses of prognostic factors for overall and disease-free survivals

	Overall survival				Disease-free survival			
	Univariate		Multivariate		Univariate		Multivariate	
	HR (95% CI)	*P*-value	HR (95% CI)	*P*-value	HR (95% CI)	*P*-value	HR (95% CI)	*P*-value
Tumor size	1.07 (0.79–1.43)	0.672			1.11 (0.86–1.45)	0.425		
Lymph node status	2.34 (1.77–3.08)	<0.001	1.46 (0.85–2.50)	0.167	2.40 (1.82–3.17)	<0.001	1.43 (0.84–2.40)	0.182
Stage	2.64 (1.90–3.69)	<0.001	1.63 (0.87–3.06)	0.128	2.77 (1.99–3.86)	<0.001	1.74 (0.95–3.20)	0.074
MIB-1 labeling index	1.46 (0.78–2.74)	0.235			1.44 (0.77–2.69)	0.250		
CDCP1 expression	4.11 (2.18–7.75)	<0.001	2.89 (1.51–5.54)	0.001	4.32 (2.31–8.08)	<0.001	3.04 (1.60–5.80)	<0.001

HR, hazard ratio; CI, confidence interval.

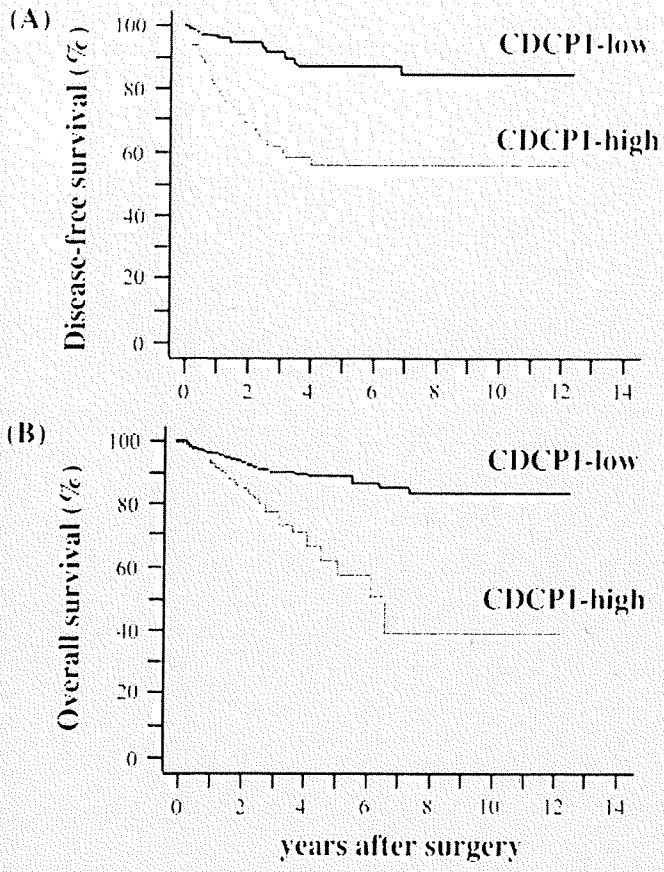

Fig. 3. Kaplan-Meier plots of disease-free (A) and overall survival (B) of patients.

The knocked-down expression of CDCP1 abolished ability of in vitro colony formation in the A549 lung adenocarcinoma cell line.[10] In addition, when injected into nude mice, the number of metastatic nodules was low in CDCP1-knocked down A549 cells as compared to parental A549 cells.[10] Taken together with the present results, CDCP1 appeared to play important roles for metastatic and tumorigenic potentials of lung adenocarcinoma not only in cell lines but also in clinical samples.

High CDCP1 expression was correlated with MIB-1 labeling index. Since the monoclonal antibody MIB-1 recognizes Ki-67 antigen that is expressed in cells during the cell cycle, except at the G0 phase, it can be applied to evaluate the proliferative activities of cells. Previously, we showed the positive correlation of CDCP1 expression with MIB-1 labeling index in breast cancer cells.[8] These findings indicate that CDCP1 expression level reflects a proliferative activity of cancer cells.

Intracellular tyrosine residues of CDCP1 are known to be phosphorylated upon activation, and the level of tyrosine phosphorylation is associated with the capacity for anchorage independence in A549 cells.[10] Immunohistochemically, phosphorylated CDCP1 was found to be localized to the peripheral areas of tumor cell nests. Lung adenocarcinoma cells often show bronchioalveolar growth in the periphery of the cancer tissues, but such portions were almost negative for phosphorylated CDCP1 expression. Phosphorylated CDCP1 was mostly present in the tumor cells expanding to the surrounding normal tissues. This was consistent with the previous report that phosphorylated CDCP1 is localized in the invasive front of gastric cancer.[12] Therefore, phosphorylated CDCP1 may play some roles for tumor invasion, in addition to anchorage independence. The staining for phosphorylated and non-phosphorylated CDCP1 demonstrated that most tumor cells expressed CDCP1 as a non-phosphorylated form. This was consistent with the report by Brown et al. that the phosphorylation of CDCP1 is dynamically balanced by Src-family kinase and phosphotyrosine phosphatase activities, yielding low equilibrium phosphorylation.[6] CDCP1 contains three extracellular CUB domains, which might be involved in cell adhesion or interaction with the extracellular matrix.[2–7] Non-phosphorylated CDCP1 may function as an adhesion molecule.

Multivariate analysis revealed the high expression of CDCP1 to be an independent factor for poor prognosis for patients with lung adenocarcinoma. Benes et al. reported that Src, which mediates proliferation signals in cancers, forms a complex with phosphorylated CDCP1.[7] These findings indicate that overexpression of CDCP1 could stimulate tumor growth, explaining why prognosis of patients with CDCP1-high tumors is worse than that with CDCP1-low tumors.

In conclusion, high CDCP1 expression is an independent factor for poor prognosis of patients with lung adenocarcinoma. Further studies will be necessary to elucidate whether CDCP1 expression could be a useful marker for prediction of prognosis in other types of cancers. CDCP1 could be a molecular target for cancer therapy.

Acknowledgments

The authors thank Ms. Megumi Sugano and Ms. Takako Sawamura for their technical assistance. This work was supported by grants from the Ministry of Education, Culture, Sports, Science and Technology, and from the Osaka Cancer Research Foundation

doi: 10.1111/j.1349-7006.2008.01066.x

References

1 Parkin DM, Bray F, Ferlay J, Pisani P. Global Cancer Statistics, 2002. CA Cancer J Clin 2005; 55: 74–108.
2 Scherl-Mostageer M, Sommergruber W, Abscher R, Hauptmann R, Ambros P, Shweifer N. Identification of a novel gene, CDCP1, overexpressed in human colorectal cancer. Oncogene 2001; 20: 4402–8.
3 Hooper JD, Zijlstra A, Aimes RT et al. Subtractive immunization using highly metastatic human tumor cells identifies SIMA135/CDCP1, a 135 kDa cell surface phosphorylated glycoprotein antigen. Oncogene 2003; 22: 1783–94.
4 Conze T, Lammers R, Kuci S et al. CDCP1 is a novel marker for hematopoietic stem cells. Ann NY Acad Sci 2003; 996: 222–6.
5 Buhring H-J, Kuci S, Conze T et al. CDCP1 identifies a broad spectrum of normal and malignant stem/progenitor cell subsets of hematopoietic and nonhematopoietic origin. Stem Cells 2004; 22: 334–43.
6 Brown TA, Yang TM, Zaitsevskaia T et al. Adhesion or plasmin regulates tyrosine phosphorylation of a novel membrane glycoprotein p80/gp140/CUB domain-containing protein 1 in epithelia. J Biol Chem 2004; 279: 14772–83.
7 Benes CH, Wu N, Elia AEH, Dharia T, Cantley LC, Soltoff SP. The C2 domain of PKC-delta is a phosphotyrosine binding domain. Cell 2005; 121: 271–80.
8 Ikeda JI, Morii E, Kimura H et al. Epigenetic regulation of the expression of the novel stem cell marker CDCP1 in cancer cells. J Pathol 2006; 210: 75–84.
9 Kimura H, Morii E, Ikeda JI et al. Role of DNA methylation for expression of novel stem cell marker CDCP1 in hematopoietic cells. Leukemia 2006; 20: 1551–6.
10 Uekita T, Jia L, Narisawa-Saito M, Yokota J, Kiyono T, Sakai R. CUB domain-containing protein 1 is a novel regulator of anoikis resistance in lung adenocarcinoma. Mol Cell Biol 2007; 27: 7649–60.
11 Sobin LH, Wittekind Ch, eds. TNM Classification of Malignant Tumors, 5th edn. New York: John Wiley & Sons, Inc., 1997.
12 Uekita T, Tanaka M, Takigahira M et al. CUB domain-containing protein 1 regulates peritoneal dissemination of gastric scirrhous carcinoma. Am J Patho 2008; 172: 1729–39.
13 Suzuki K, Nagai K, Yoshida J et al. Conventional Clinicopathologic Prognostic Factors in Surgically Resected Nonsmall Cell Lung Carcinoma. Cancer 1999; 86: 1976–84.

Oncogene (2009) 28, 662-673

www.nature.com/onc

ORIGINAL ARTICLE

Distinct role of ShcC docking protein in the differentiation of neuroblastoma

I Miyake[1], M Ohira[2], A Nakagawara[2] and R Sakai[1]

[1]*Growth Factor Division, National Cancer Center Research Institute, Tokyo, Japan and* [2]*Division of Biochemistry, Chiba Cancer Center Research Institute, Chiba, Japan*

The biological and clinical heterogeneity of neuroblastoma is closely associated with signaling pathways that control cellular characteristics such as proliferation, survival and differentiation. The Shc family of docking proteins is important in these pathways by mediating cellular signaling. In this study, we analysed the expression levels of ShcA and ShcC proteins in 46 neuroblastoma samples and showed that a significantly higher level of ShcC protein is observed in neuroblastomas with poor prognostic factors such as advanced stage and *MYCN* amplification ($P<0.005$), whereas the expression level of ShcA showed no significant association with these factors. Using TNB1 cells that express a high level of ShcC protein, it was demonstrated that knockdown of ShcC by RNAi caused elevation in the phosphorylation of ShcA, which resulted in sustained extracellular signal-regulated kinase activation and neurite outgrowth. The neurites induced by ShcC knockdown expressed several markers of neuronal differentiation suggesting that the expression of ShcC potentially has a function in inhibiting the differentiation of neuroblastoma cells. In addition, marked suppression of *in vivo* tumorigenicity of TNB1 cells in nude mice was observed by stable knockdown of ShcC protein. These findings indicate that ShcC is a therapeutic target that might induce differentiation in the aggressive type of neuroblastomas.
Oncogene (2009) **28,** 662–673; doi:10.1038/onc.2008.413; published online 10 November 2008

Keywords: Shc family; ERK; neuroblastoma; differentiation; RNAi

Introduction

Neuroblastoma is the most common pediatric solid tumor derived from the sympathoadrenal lineage of neural crest and its clinical and biological features are heterogeneous. Some types of neuroblastomas show favorable outcomes with spontaneous differentiation or regression by minimum treatment, whereas other types have malignant characteristics with metastasis and resistance to chemotherapy. Age of onset, tumor volume, presence of metastasis, pathological features and amplification of the *N-myc* gene are important prognostic factors of neuroblastoma. Previously, it was reported that the differential expression of Trk family receptors might contribute to clinical and biological outcomes of neuroblastomas (Nakagawara *et al.*, 1993; Nakagawara and Brodeur, 1997) whereas the cellular signaling involved in the regulation of the aggressiveness of neuroblastoma is largely unknown.

The Shc family of docking proteins is important in signaling pathways mediating the activation of various receptor tyrosine kinases (RTKs) such as the Trk family triggered by extracellular stimulations, to specific downstream molecules. The Ras–extracellular signal-regulated kinase (ERK) pathway and the phosphoinositide-3 kinase (PI3K)–Akt pathway are the most common signals regulated by Shc family proteins, representing important functions in cellular proliferation, survival and differentiation.

The Shc family has three members, ShcA/Shc, ShcB/Sli/Sck and ShcC/Rai/N-Shc encoded by different genes (Nakamura *et al.*, 1996; O'Bryan *et al.*, 1996; Pelicci *et al.*, 1996). ShcA protein having three protein isoforms, p46, p52 and p66, is ubiquitously expressed in most organs except the adult neural systems, whereas ShcC (p52 and p67 isoforms) are exclusively expressed in the neuronal system (Sakai *et al.*, 2000). In the central nervous system, ShcA expression is most significant during embryonic development with sudden decrease after birth. On the other hand, ShcC expression is remarkably induced around birth and maintained in the mature brain. The Shc family molecules have a unique PTB–CH1–SH2 modular organization with two phosphotyrosine-binding modules, PTB and SH2 domains, which recognize various phosphotyrosine-containing peptides with different specificities. CH1 domains contain several tyrosine phosphorylation sites that recruit other adaptor molecules such as Grb2. Functional analysis of ShcB and ShcC on the neuronal signal pathway indicate that these proteins in neuronal cells potentially regulate epidermal growth factor (EGF) or nerve growth factor (NGF) signaling in a similar fashion to ShcA (O'Bryan *et al.*, 1996; Nakamura *et al.*, 1998).

Major parts of neuroblastoma cell lines show the expression and tyrosine phosphorylation of ShcC protein, but its effect on the biology of tumor cells

Correspondence: Dr R Sakai, Growth factor Division, National Cancer Center Research Institute, Tsukiji, Chuo-ku, Tokyo 104-0045, Japan. E-mail: rsakai@ncc.go.jp
Received 9 May 2008; revised 3 September 2008; accepted 1 October 2008; published online 10 November 2008

remains to be elucidated. We have recently shown that constitutive tyrosine phosphorylation of ShcC is induced in a subset of neuroblastoma cells by the activation of anaplastic lymphoma kinase (ALK) owing to *ALK* gene amplification and the constitutively activated ALK–ShcC signal pathway could induce cell survival, anchorage-independent growth of the cells and progression of tumors (Miyake *et al*., 2002, 2005). In our study, significant amplification of *ALK* was observed in 3 of 13 neuroblastoma cell lines and in only 1 of 85 cases of human neuroblastoma samples (Osajima-Hakomori *et al*., 2005). Considering these results, it was suspected ShcC might also contribute to the signal pathway associated with the tumor behavior in ALK-independent manners in majority of neuroblastoma cells.

In a recent report, high expression of ShcC mRNA was shown to be a poor prognostic factor in neuroblastoma patients through the semiquantitative reverse transcriptase -PCR analysis of tissue samples (Terui *et al*., 2005), suggesting the possibility that ShcC protein might be causative of tumor progression in neuroblastoma patients. In the current study, we examined the expression levels of ShcC protein in tumor samples of 46 neuroblastoma patients and confirmed the significant association of the expression levels of ShcC protein with several factors linked to unfavorable outcome of neuroblastoma. Furthermore, we investigated the functions of ShcC in cell proliferation, differentiation and *in vivo* tumorigenicity of neuroblastoma cells by knockdown of ShcC expression in neuroblastoma cell lines expressing a high level of ShcC without *ALK* amplification.

Results

Expression and tyrosine phosphorylation of ShcC in neuroblastoma cell lines

At first, the expression of ShcA and ShcC was analysed in 11 neuroblastoma cell lines using each specific antibody (Supplementary Figure A) along with DLD-1 as a control, which is known to express ShcA protein (mainly p46ShcA and p52ShcA), but not ShcC protein (Figure 1a). The three cell lines with *ALK* gene amplification (NB-39-v, Nagai and NB-1: Group A) expressed ShcC at a moderate level in contrast to their significant phosphorylation so that ALK–ShcC complex is mediating the dominant oncogenic signal (Miyake *et al*., 2002; Osajima-Hakomori *et al*., 2005). Other

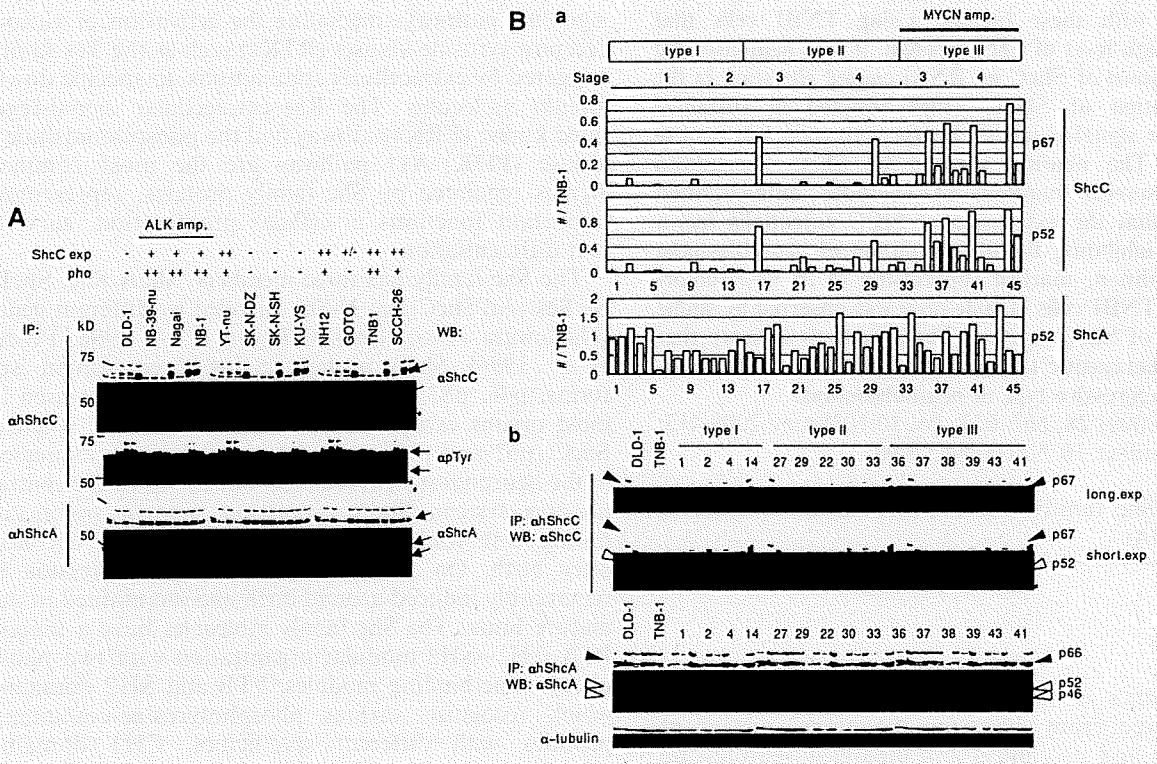

Figure 1 (**A**) Expression and tyrosine phosphorylation of ShcC in neuroblastoma cell lines detected by specific antibody. The expression of ShcA (lower panel), ShcC (upper panel) and tyrosine phosphorylation of ShcC was analysed in 11 neuroblastoma cell lines including the cell lines with anaplastic lymphoma kinase (*ALK*) gene amplification (*ALK* amp.) along with DLD-1 as a control. Lysates were immunoprecipitated and then immunoblotted with antibodies against the indicated molecules. The levels of expression/phosphorylation of ShcC are indicated above. Asterisks show heavy chains of immunoglobulin. Positions of molecular mass markers (kDa) are shown to the left. (**B**) Expression of ShcC and ShcA in the tissue samples of three subsets of neuroblastoma patients. (a) Expression levels of ShcC/ShcA in the samples of 46 neuroblastoma patients were detected by western blotting being compared to the level of expression in TNB-1 cells (=1.0) as an internal control among each experiment and was corrected by each expression level of a-tubulin. (b) Expression of ShcC (upper panel)/ShcA (middle panel) of representative samples of each subset were detected on a filter. The exposure time of the filter onto X-ray films was different to detect between p52ShcC (short exposure: lower panel) and p67ShcC (long exposure: upper panel). Each isoform of ShcC/ShcA is indicated by opened or filled triangles. Asterisks show heavy chains of immunoglobulin.

neuroblastoma cells with a single copy of the *ALK* gene were divided into two groups, one with considerably high levels of ShcC expression (YT-v, NH-12, TNB-1 and SCCH-26: Group B) and the other with almost no ShcC expression (KU-YS, SK-N-DZ, SK-N-SH and GOTO: Group C). Most of the cells in the Group B showed a morphological tendency to aggregate each other and rather low adhesion to the culture plate, compared with the cells of the Group C (data not shown). The degrees of ShcC phosphorylation in the cells in Group B appeared to be lower than the cells with *ALK* amplification (Figure 1A, middle panel). In contrast to ShcC, the expression of ShcA was within similar levels among neuroblastoma cell lines (Figure 1A, lower panel).

The expression level of ShcC is prominent in tissue samples of poor risk neuroblastoma patients

Next we analysed the expression of ShcA and ShcC protein in 46 primary human neuroblastoma specimens using each specific antibody. These tissue samples were classified into three subsets using Brodeur's classification; type I (stage 1, 2 or 4S; a single copy of *MYCN*), type II (stage 3 or 4; a single copy of *MYCN*) and type III (all stages; amplification of *MYCN*) (Brodeur and Nakagawara, 1992; Ohira *et al*., 2003). The expression level of ShcA and ShcC in western blotting was standardized by intensity of α-tubulin within each filter, standardized by the amounts in TNB-1 cells as an internal control among different filters and statistically evaluated from at least two independent western blots for each sample (Table 1). We found that there is a significant difference in the expression levels of ShcC among the subsets of neuroblastomas. In the group of type II and type III, the expression level of ShcC protein was substantially higher than that in the type I group (Figure 1Ba). Both isoforms of ShcC, p52ShcC and p67ShcC, showed similar patterns of expression. As shown in Table 2, the expression level of ShcC has a significant correlation with several clinical factors including late onset of the disease (later than 12 months) (p52/p67: $P<0.001/P=0.015$), advanced clinical stage (stages III and IV) ($P<0.001$) and gene amplification of *MYCN* (p52/p67: $P<0.002/P=0.005$). Furthermore, most of the samples from the patients who died within 12 months after the onset of the disease showed significantly higher levels of ShcC expression than the other group of samples in which patients lived longer than 12 months (p52/p67: $P=0.006/P=0.009$). In contrast, variable expression levels of both isoforms of ShcA protein, p52 and p66, were observed in neuroblastoma samples with no significant difference among three subsets of clinical group ($P>0.05$) (Table 2; Figure 1Ba). The results of representative samples from each subset are shown in Figure 1Bb. These data indicate that the expression of ShcC protein is significantly associated with multiple prognostic factors of neuroblastoma, suggesting that ShcC has specific functions in malignant phenotypes of neuroblastoma presumably by modulating cellular signaling.

Biological effects of ShcC downregulation on TNB-1 cells

To elucidate the biological functions of ShcC in the tumor characteristics causing unfavorable outcomes of neuroblastoma patients, we investigated the effects of ShcC knockdown on the cellular biology and signal transduction in one of the neuroblastoma cell lines, TNB-1, which expresses a high level of ShcC protein with no *ALK* amplification. The expression of ShcC and ShcA was suppressed by RNA interference using two independent sets of specific small interfering RNA (siRNA) oligonucleotides corresponding to ShcC and ShcA, respectively (Figure 2Aa). The growth rate of TNB-1 cells transfected with the ShcA siRNA was severely suppressed (Figure 2Ab), owing to impaired ability of proliferation and survival, which is consistent with previous reports (Ravichandran, 2001). ShcC-knockdown cells showed a relatively weak effect on growth rate in the normal culture condition (Figure 2Ab).

Downregulation of ShcC induces neurite outgrowth and increases differentiation-related markers in TNB-1 cells

ShcC knockdown caused morphological changes to rather flat and spindle shape and neurite extension within 24 h after transfection of ShcC siRNA (Figure 2Ba). These neurite-bearing cells express higher amount of microtubule-associated protein 2 (MAP-2), growth-associated protein 43 (GAP-43), a protein expressed in the growing neurites, and chromogranin A (Chr-A; Figure 2Bb), markers of neuronal differentiation (Giudici *et al*., 1992) than the control cells. On the other hand, TNB-1 cells treated with ShcA siRNAs showed no remarkable change compared with the control cells, relatively round with small processes attached to the dish surface (Figure 2Ba). These results suggest that the endogenous ShcC negatively affects neurite outgrowth and differentiation of TNB-1 cells.

Persistent activation of ERK1/2 due to ShcC downregulation induces neurite outgrowth in TNB-1 cells

Neuronal differentiation is closely associated with mitogen-activated protein kinase (MAPK)/ERK kinase (MEK)/ERK and PI3K–AKT pathways and both of them might be controlled downstream of Shc family signaling. Downregulation of ShcA induced the suppression of extracellular signal-related kinase 1/2 (ERK1/2) and AKT pathways at 48 h after transfection of siRNA, nevertheless ShcC downregulation apparently elevated the base level of ERK phosphorylation and slightly enhanced AKT activation (Figure 3a). This elevation of ERK phosphorylation sustained until 96 h after transfection of siRNA. Similar effect on the ERK activation was also observed in NH-12 and YT-v cells, which express high amount of ShcC (Supplementary Figure B). It is reported that sustained activation of ERK is responsible for neurite outgrowth and differentiation of PC12 cells (Qui and Green, 1992). To investigate whether neuronal extension of TNB-1 cells by ShcC RNAi was induced by sustained activation of ERK, the effect of MEK inhibitor, PD98059, on the

Table 1 Characteristics of 46 neuroblastoma samples

Case	*Type*	*Stage*	*Age (months)*	*MYCN*	*Prognosis*	*p52ShcC*	*p67ShcC*	*p52ShcA*	*p66ShcA*
1	I	1	8	1	A	0.01	0	0.92	0.58
2		1	7	1	A	0	0	0.92	0.52
3		1	8	1	A	0.13	0.07	1.16	0.58
4		1	1	1	A	0	0	0.81	0.63
5		1	4	1	A	0.013	0	1.26	0.62
6		1	8	1	A	0.03	0.006	0.81	0.60
7		1	8	1	A	0	0	0.54	0.70
8		1	7	1	A	0	0	0.40	0.48
9		1	9	1	A	0	0	0.40	0.58
10		1	7	1	A	0.15	0.05	0.42	0.31
11		1	7	1	A	0.003	0	0.35	0.36
12		2	38	1	A	0.047	0	0.41	0.20
13		2	7	1	A	0	0	0.40	0.39
14		2	7	1	A	0.038	0	0.60	0.63
15		2	> 132	1	A	0.03	0	0.83	0.62
16	II	3	8	1	A	0	0	0.56	0.45
17		3	7	1	A	0.72	0.45	0.42	0.49
18		3	7	1	A	0.03	0.01	1.2	0.62
19		3	8	1	A	0.015	0.01	1.3	0.67
20		3	23	1	A	0	0	0.25	0.32
21		3	22	1	A	0.10	0	0.63	0.63
22		3	> 108	1	A	0.23	0.03	0.45	0.36
23		3	18	1	A	0.074	0.025	0.75	0.45
24		3	47	1	A*	0	0.03	0.87	0.65
25		3	21	1	D	0.089	0.03	0.76	0.56
26		3	96	1	A*	0.054	0.001	1.6	0.54
27		4	5	1	A	0.03	0	1.03	0.28
28		4	55	1	A	0.22	0.018	1.14	0.33
29		4	4	1	A	0	0	0.52	0.49
30		4	22	1	D	0.49	0.43	0.89	0.48
31		4	45	1	A*	0	0.068	1.17	0.53
32		4	57	1	A*	0.10	0.093	1.2	0.42
33		4	102	1	A*	0.15	0	1.5	0.49
34	III	3	32	amp	A*	0	0	1.6	0.37
35		3	13	amp	D	0.11	0.10	0.86	0.53
36		3	33	amp	D	0.77	0.50	0.64	0.50
37		3	21	amp	A*	0.47	0.18	0.47	0.49
38		3	26	amp	A*	0.84	0.57	1.1	0.58
39		4	23	amp	D	0.38	0.13	0.99	0.35
40		4	7	amp	D	0.25	0.15	1.1	0.58
41		4	> 132	amp	D	0.96	0.55	1.32	0.65
42		4	18	amp	D	0.22	0.13	0.99	0.63
43		4	> 24	amp	D	0.10	0	0.76	0.54
44		4	59	amp	D	0	0	1.80	0.85
45		4	30	amp	D	0.99	0.76	0.60	0.56
46		4	34	amp	D	0.56	0.21	0.53	0.47

Type, as described in 'Materials and methods'; age: onset of the disease (months); stage, INSS stage; MYCN, single copy (1) or amplification (amp) of *MYCN* gene; prognosis, alive (A) or death (D) within 12 months after diagnosis; A*, death after 12 months from diagnosis; p52/p67 ShcC and p52/66 ShcA, the intensity of each band obtained by western analysis, standardized according to control signals, such as the bands of TNB-1 and α-tubulin as described in 'Materials and methods'.

differentiation of TNB-1 cells by knockdown of ShcC was examined. It was found that inhibition of the ERK pathway abolished the neurite outgrowth of TNB-1 cells by ShcC knockdown, indicating that ShcC protein has the potential to suppress neurite outgrowth which is dependent on the sustained activation of the ERK pathway (Figure 3b). In addition, the sustained activation of ERK by the expression of activated Raf protein, RafCAAX (Leevers *et al*., 1994; Stokoe *et al*., 1994) also induced neurite outgrowth in TNB-1 cells (Supplementary Figure C) just as in PC12 cells (Dhillon *et al*., 2003). We also analysed the effect of PI3K inhibitor on neurite outgrowth induced by ShcC RNAi to check the involvement of the PI3K–AKT pathway, whereas no apparent effects on the number and length of the neurite extension were observed (Supplementary Figure D).

Effect of ShcC knockdown on ERK activation is enhanced by collagen stimulation by ShcA–Grb2 signaling

Among several culture conditions of cells examined for the effect of ShcC RNAi on the activity of ERK, the most obvious activation of ERK was observed after the

Table 2 Correlation between the expression of ShcC protein and identified prognostic factors of neuroblastoma

	p52		*p67*	
	Average	*t-Test*	*Average*	*t-Test*
ShcC				
Age (months)				
12>	0.071		0.037	
>12	0.27	**<0.001**	0.18	0.015
Stage				
I–II	0.03		0.0084	
III–IV	0.26	**<0.001**	0.14	**<0.001**
MYCN				
Single	0.083		0.040	
amp.	0.43	**0.002**	0.25	**0.005**
Death in 12 months				
–	0.10		0.047	
+	0.41	**0.006**	0.25	**0.009**
	p52		*p66*	
	Average	*t-Test*	*Average*	*t-Test*
ShcA				
Age (months)				
12>	0.72		0.53	
>12	0.82	0.2	0.52	0.32
Stage				
I–II	0.68		0.52	
III–IV	0.82	0.1	0.52	0.22
MYCN				
Single	0.73		0.51	
amp.	0.88	0.16	0.55	0.16
Death in 12 months				
–	0.75		0.50	
+	0.84	0.27	0.57	0.11

Expression levels of ShcC and ShcA in tissue samples from 46 neuroblastoma patients quantified were analyzed statistically using *t*-test. The variables compared are age, onset of the disease (months); stage, INSS stage; MYCN, single copy or amplification of *MYCN* gene. Statistically significant correlation ($P<0.01$) is indicated in bold.

cells were plated on collagen dishes following suspending condition (Figure 4a, lower panel). On the contrary, the activation level of ERK due to ShcC RNAi was not significant in the suspending condition (Supplementary Figure E, left panel) showing that ShcC RNAi-induced ERK activation depends on attachment to the specific extracellular matrix (ECM).

In contrast, ERK activation was consistently suppressed by knockdown of ShcA regardless of these culture conditions (Figure 4a, upper panel).

Integrins-mediated extracellular signaling lead the activation of Ras/ERK signaling by ShcA, and that process is reported to be associated with Src family kinase (Wary *et al*., 1996, 1998), focal adhesion kinase (Hecker *et al*., 2002) or some RTKs (Moro *et al*., 1998; Hinsby *et al*., 2004). In TNB-1 cells, enhanced ShcA phosphorylation and ShcA–Grb2 complex formation was observed following collagen stimulation and further increased by ShcC RNAi (Figures 4b and c). To examine whether the phosphorylation of ShcA is necessary for the neurite formation, the effect of double knockdown of both ShcC and ShcA was examined in TNB-1 cells. ERK activation and neurite outgrowth were not detected in the absence of both ShcC and ShcA, indicating that ShcC RNAi-induced neurite outgrowth of TNB-1 cells might be dependent on the ShcA expression in adherent state (Figure 4d).

Expression of ShcC suppresses the phosphorylation of ShcA in KU-YS cells stimulated by EGF

To further analyse the effects of ShcC expression on ShcA phosphorylation in neuroblastoma cells, we introduced a vector expressing p52ShcC into KU-YS neuroblastoma cells, which do not express a detectable amount of endogenous ShcC protein (Figure 1A), and obtained several stable clones expressing p52ShcC at different levels (Figure 5a). As controls, clones overexpressing p46/p52ShcA, or expressing the expression vector alone were also prepared. We checked the ShcA phosphorylation of each clone under the stimulation of EGF (Figure 5b). EGF stimulation to the control and ShcA expressing cells showed typical activation of ShcA, whereas the cell expressing ShcC showed decreased levels of ShcA phosphorylation according to the levels of ShcC protein. We also confirmed that activation of ShcA by EGF was suppressed in the cells transiently overexpressing ShcC (Supplementary Figure F). Those cells showed almost the same level of EGF receptor (EGFR) activation induced by EGF, judging from the phosphorylation levels of EGFR indicating that the expression of ShcC negatively affected the EGFR–ShcA signaling after the activation of EGFR, such as competing manners against ShcA. In addition, we examined whether tyrosine phosphorylation of ShcC is crucial for the suppression of ShcA phosphorylation by establishing two clones that express a p52ShcC mutant, 3YF lacking all three tyrosines, which are reported to be involved in the tyrosine phosphorylation of ShcC (Miyake *et al*., 2005). It was revealed that the 3YF mutant of ShcC could suppress the EGF-induced activation of ShcA in both clones almost as efficiently as the original ShcC in ShcC2 cells (Supplementary Figure G), suggesting that negative regulation of ShcA phosphorylation by ShcC does not require tyrosine phosphorylation of ShcC.

ShcC downregulation negatively affects anchorage-independent growth and in vivo *tumorigenicity*

We investigated the effect of ShcC knockdown on the anchorage-independent growth and *in vivo* tumorigenicity of TNB-1 cells by establishing cells with stable suppression of ShcC expression using the miR RNAi expression vector (as described in 'Materials and methods'). As analysed in the mixed clones by soft agar colony formation assay, stable suppression of ShcC caused marked inhibition of anchorage-independent growth (Figure 6a). Three isolated clones of ShcC miR

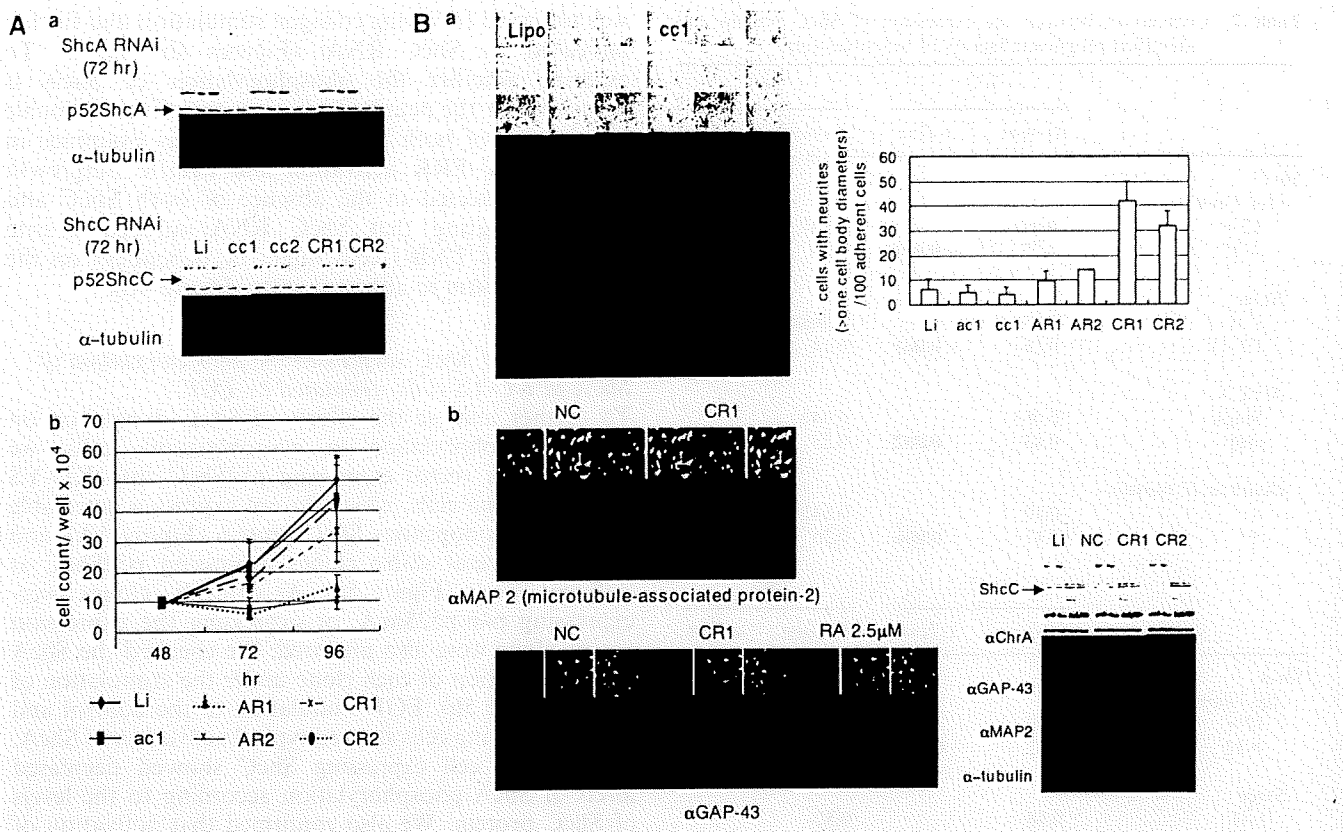

Figure 2 Biological effects of ShcC downregulation using small interfering RNA (siRNA) on TNB-1 cells. (**A**) (a) Expression of ShcC (lower panel) and ShcA (upper panel) was suppressed by RNA interference using specific siRNA oligonucleotides corresponding to ShcC and ShcA, respectively, then, detected by western analysis with each specific antibody. (b) Growth rate of siRNA-treated cells in tissue culture condition. TNB-1 cells 48 h after the transfection with ShcA/ShcC siRNA cultured by 30-mm dishes were counted at the indicated time points. The results represent the average values (±s.d.) of three replicated experiments. (**B**) Downregulation of ShcC induces neurite outgrowth and increases the expression of differentiation-related markers in TNB-1 cells. (a) Evaluation of neurite outgrowth of ShcA or ShcC-knockdown TNB-1 cells 72 h after siRNA treatment without any extracellular matrix (ECM) stimulation. (b) Expression of several molecules used as differentiation-related markers in ShcC-knockdown TNB-1 cells (left panel: immunostaining of neuritis as described in 'Materials and methods'; right panel: western analysis using indicated antibodies). As a positive control of differentiation, 2.5 μM retinoic acid (RA) was treated 24 h before analysis. AR1, AR2/CR1, CR2: two independent siRNA of ShcA /ShcC; Li: treated with only Lipofectamine 2000; ac1, ac2/cc1, cc2: control siRNA for ShcA /ShcC siRNA, respectively. NC: negative control for universal siRNA (as described in 'Materials and methods').

RNAi (miShcC-1, -2 and -3) were prepared by checking the level of ShcC protein along with clones of LacZ miR RNAi (miLacZ-1 and -2) as controls (Figure 6b). These clones with suppressed level of ShcC showed the same morphological features of neurite formation in tissue culture condition as observed in the cells transfected with ShcC siRNAs (data not shown). The volumes and weights of subcutaneous tumors in nude mice were measured at 6 weeks after injections of the cells and evaluated in at least 4 independent injections per clone. Control LacZ miR RNAi clones (miLacZ-1, miLacZ-2) developed large tumor masses *in vivo* (Figure 6c), whereas remarkable reduction of the size and weight of tumors (or almost disappearance of tumors in some cases) was observed by the stable suppression of ShcC expression. These tumors from ShcC miR RNAi clones showed marked increase in numbers of apoptotic cells compared with control tissues as shown by terminal transferase dUTP nick-end labeling (TUNEL) staining. On the other hand, staining by a proliferation marker, Ki-67 showed no significant difference among each tumor tissue (Figure 6d).

Discussion

It has already been shown that some signal pathways strongly affect tumor progression and treatment resistance (Schwab *et al*., 2003). Other than the Trk family, the PI3K/Akt pathway (Opel *et al*., 2007), Ret (Iwamoto *et al*., 1993; Marshall *et al*., 1997), hepatocyte growth factor/c-Met pathway (Hecht *et al*., 2004) were reported to be closely associated with several diagnostic profiles and biological characteristics of neuroblastoma cells.

This is the first study to show that the expression of ShcC protein, a member of the Shc family docking proteins, is significantly correlated with malignant phenotypes associated with advanced neuroblastoma. Expression of both p52 and p67 isoforms of ShcC,

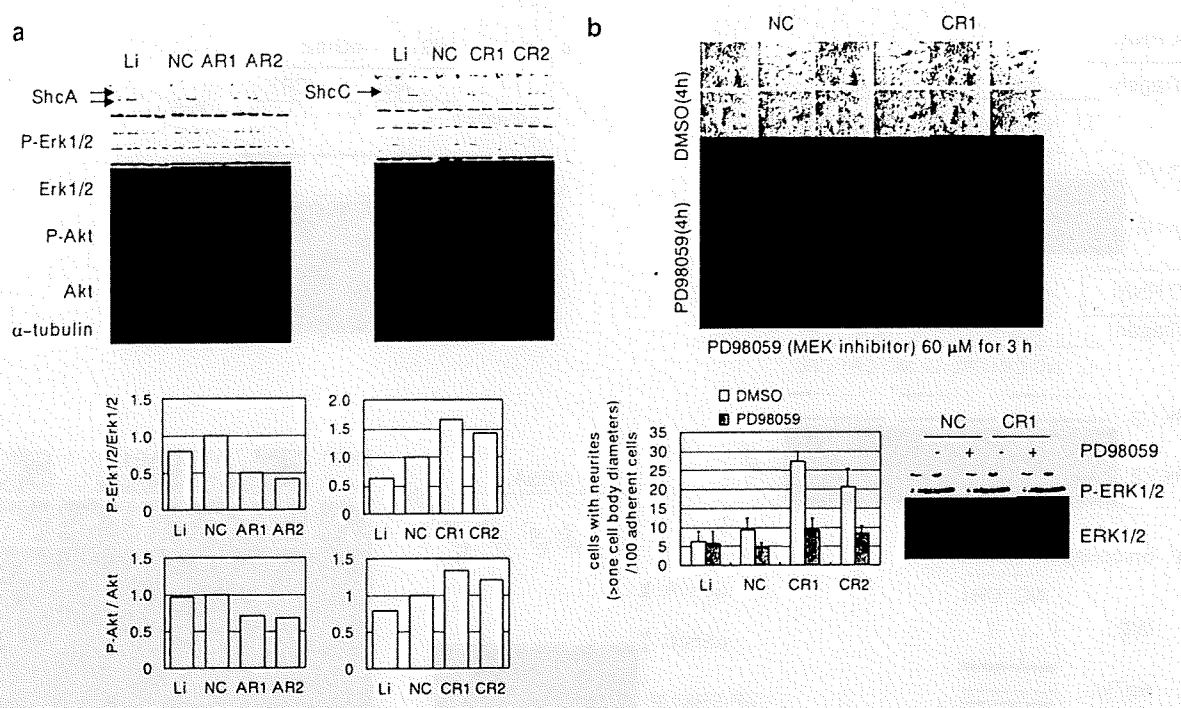

Figure 3 Persistent activation of extracellular signal-related kinase 1 2 (ERK1/2) in ShcC downregulation induces neurite outgrowth in TNB-1 cells. (**a**) Downregulation of ShcC positively affects the ERK1/2 and Akt pathway in TNB-1 cells. Activation of ERK1/2 and Akt in the cells treated with ShcA or ShcC siRNA were examined by western blotting. The levels of activation were quantified comparing to that of cells treated with control siRNA (NC). (**b**) Effect of MEK inhibitor on neurite outgrowth induced by ShcC RNAi in TNB-1 cells. The siRNA-transfected cells indicated were treated with dimethylsulphoxide (DMSO) or PD98059 and incubated for 3 h in the tissue culture condition, then counted for neurite-containing cells.

shows significant correlation with clinical stage and *MYCN* gene amplification whereas the expression of both isoforms of ShcA, p52 and p66, showed little association with those aspects. These results, in the protein level, give further evidence that ShcC is a factor which determines the prognosis of neuroblastoma, which was recently suggested by analysis of the mRNA expression of ShcC (Terui *et al*., 2005).

The biological analysis of TNB-1 cells treated with ShcC-specific siRNAs provided evidence that ShcC protein expressed in the neuroblastoma cells is suppressing the differentiation of neuroblastoma cells. Neurite outgrowth of TNB-1 cells, induced by downregulation of ShcC was dependent on sustained activation of the MEK/ERK pathway. Sustained activation of the ERK pathway triggered by factors such as NGF is required for neuronal differentiation in some neuronal tumor cells such as PC12 cells (Qui and Green, 1992; Yaka *et al*., 1998). The fact that constitutively activated Raf–ERK signaling induced neurite outgrowth in the same cell line (Supplementary Figure C), such as the RTK-related pathway might induce the ERK activation and cellular differentiation in TNB-1 cells, although NGF stimulation failed to induce neurite elongation of TNB-1 cells (data not shown).

Interestingly, elevation in the level of phosphorylated ShcA followed by activation of the ERK pathway by ShcA–Grb2 signals was observed in TNB1 when the ShcC protein expression was suppressed by RNAi. This activation of the ShcA–Grb2–ERK pathway caused by downregulation of ShcC may be due to a competitive effect between ShcC and ShcA for binding to certain RTKs. This possibility is supported by another experiment showing that both EGF-induced phosphorylation of ShcA and complex formation between ShcA and Grb2 in KU-YS cells are suppressed by the expression of ShcC in a dose-dependent manner. It was shown that the expression of the PTB domains of ShcC partially interfered with the binding of endogenous ShcA to activated EGFR in 293 cells (O'Bryan *et al*., 1998). These data are consistent with our current findings described above. It is suspected that some types of differentiation signals mediated by ShcA are blocked by the overexpression of ShcC in some neuroblastoma cells such as TNB-1, and the suppression of ShcC protein by RNAi causes the ShcA-mediated differentiation of these cells.

Elevated level of ShcA phosphorylation and ERK activation induced by ShcC downregulation was more significant under the stimulation of collagen I than without any ECM stimulation. In addition, in suspending condition we could not detect any activation of ShcA nor ERK signal after ShcC downregulation (Supplementary Figure E). These results indicate that the difference between ShcA and ShcC might be in interaction with matrix-adhesion signals. ShcA is considered to be implicated in the adherent related pathway, phosphorylated by forming a complex with

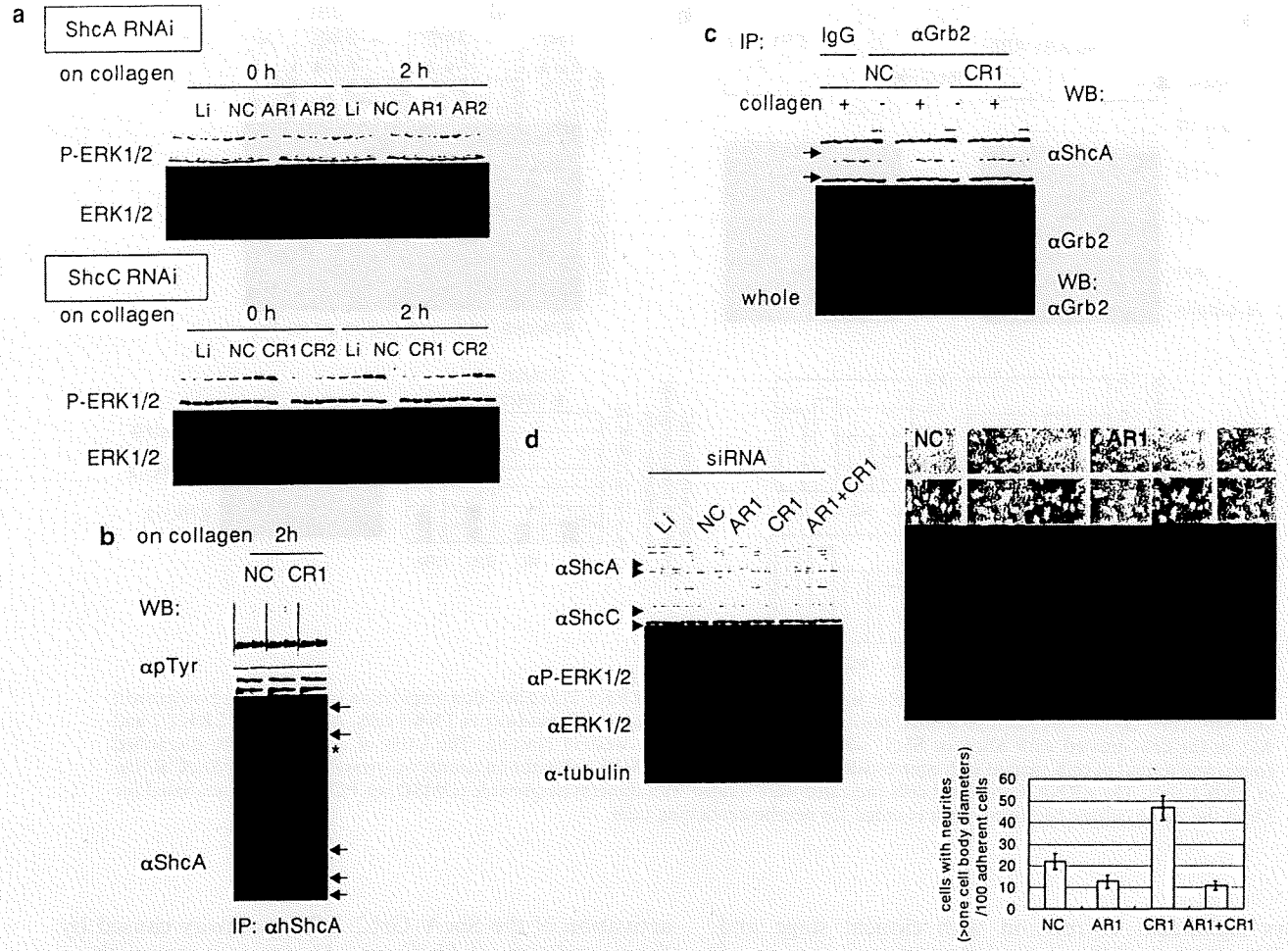

Figure 4 Elevation of extracellular signal-regulated kinase ()-activated level in ShcC-knockdown cells is increased by collagen stimulation by ShcA–Grb2 signaling. (**a**) Elevation of the ERK1/2-activated level due to ShcC downregulation is further increased 2 h after collagen stimulation. siRNAs of ShcA/ShcC-transfected TNB-1 cells (AR1, AR2/CR1, CR2, respectively) were incubated in the tissue culture condition for 70 h and stimulated by collagen type 1. Duplicated cells were harvested 0 and 2 h after collagen stimulation (as described in 'Materials and methods'). (**b**) After collagen stimulation ShcA was phosphorylated more strongly in ShcC-knockdown cells than the control cells. Asterisks show heavy chains of immunoglobulin. (**c**) ShcA–Grb2 complex formation (upper panel) were increased by downregulation of ShcC. (**d**) The ShcA-knockdown effect on the neurite outgrowth in cells transfected with ShcC siRNA was evaluated by the same method performed in Figure 2Ba. The number of neurites observed in the cells transfected with both ShcA and ShcC siRNA was obviously decreased compared to cells transfected with only ShcC siRNA.

Fyn (Wary *et al*., 1998) through its proline-rich region that is not conserved in ShcC.

In tissue culture and in transgenic mice, signaling through Fyn has been closely associated with neurite extension and cell adhesion (Brouns *et al*., 2000, 2001). Berwanger *et al*. (2002) referred to the inverse correlation between the expression of Fyn and progression of neuroblastoma from 94 primary neuroblastoma specimens, showing that expressed Fyn-induced differentiation and growth arrest of neuroblastoma cell lines. Another report indicated that active Fyn kinase induces a lasting activation of the MAPK pathway through inhibition of MAPK phosphatase 1 (Wellbrock *et al*., 2002). We confirmed that neurite outgrowth of ShcC-knockdown TNB-1 cells was suppressed by Src family inhibitor, PP2 (Supplementary Figure H). These data suggest the possibility that Integrin–Fyn–ShcA signals could be closely associated with the differentiation of TNB-1 cells induced by ShcC downregulation along with the signals of RTK–ShcA/ShcC.

Noticeably, the interference of the ShcA-mediated signaling by ShcC protein is independent of tyrosine phosphorylation of ShcC. The function of the nonphosphorylated domain of ShcC such as SH2 might be also highlighted. As for the difference in the downstream signaling between ShcC and ShcA, little is known so far. Regarding to this point, Nakamura *et al*. (2002) indicated that inhibition of NGF-induced ERK activation by the expression of ShcC was due to the different Grb2-binding capacity between ShcA and ShcC in response to NGF. It was previously reported that ShcA preferentially binds to TrkA (Yamada *et al*., 2002), which is the key receptor against NGF due to neurite outgrowth with the sustained ERK phosphorylation,

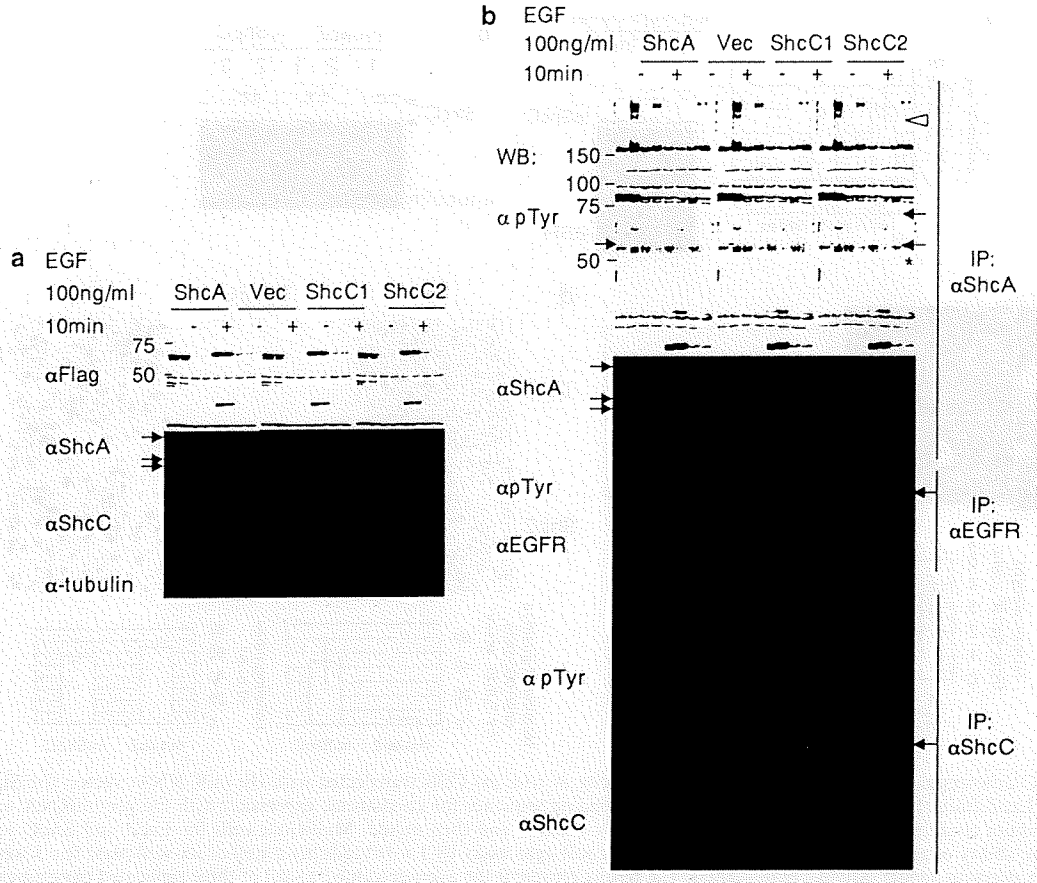

Figure 5 High expression of ShcC suppresses the phosphorylation of ShcA in KU-YS cells stimulated by epidermal growth factor (EGF). We generated stable clones of KU-YS cells expressing Flag-tagged ShcA and diverse levels of p52ShcC (ShcC1 and ShcC2) other than clones transfected with the control vector. (**a**) Each expression level was detected by western analysis. (**b**) Levels of expression and tyrosine phosphorylation of EGFR (middle panel), ShcA (upper panel) and ShcC (lower panel) were analysed by immunoprecipitation and immunoblotting using the antibodies indicated in figure in the KU-YS clone cells stimulated by EGF (as described in 'Materials and methods'). Asterisks show heavy chains of immunoglobulin.

whereas ShcC associated with TrkB rather than TrkA (O'Bryan *et al*., 1998; Liu and Meakin, 2002). In neuroblastoma, the function of signal pathways downstream of these two neurotrophin receptors might be quite different (Nakagawara *et al*., 1993), also suggesting the distinct function of downstream signal mediated by ShcC.

The effect of ShcC knockdown in *in vivo* tumorigenicity was quite remarkable comparing the effect in growth rate in tissue culture condition. We found that anchorage-independent growth in cells was also dramatically decreased by knockdown of ShcC as shown by soft agar assay (Figure 6a). Furthermore, the proportion of apoptotic cells in the nude mouse tumors generated from neuroblastoma cells *in vivo* was remarkably increased by the knockdown of ShcC. In recent study, Magrassi *et al*. (2005) showed that ShcC positively effects on cell survival by PI3K–AKT pathway in glioma cells using dominant negative form of ShcC. Theses data indicate that ShcC has additional function in the protection from some types of apoptosis in addition to the induction of differentiation of cells.

It was indicated that ShcC might have a potent function for tumor progression in neuroblastoma by suppressing the differentiation and by promoting the anchorage-independent growth in the majority of neuroblastoma cells which has high expression of ShcC protein. From these points of view, we suggest that ShcC is a potent tool for predicting the phenotype of neuroblastoma and is also a good candidate for therapeutic targets of advanced neuroblastoma.

Materials and methods

Cell culture and tissue samples

DLD-1 cells and all cell lines of neuroblastomas in this study were prepared as described in the previous report (Miyake *et al*., 2002). These cells were cultured in an RPMI 1640 medium with 10% fetal calf serum (FCS) (Sigma, St Louis, MO, USA) at 37 °C in an atmosphere containing 5% CO_2.

Anonymous 46 frozen neuroblastoma tissues were used in this study. The samples were divided into three subsets using Brodeur's classification; type I (stage 1, 2 or 4S; a single copy of *MYCN*), type II (stage 3 or 4; a single copy of *MYCN*) and type III (all stages; amplification of *MYCN*) (Brodeur and Nakagawara, 1992; Ohira *et al*., 2003). A total of 15 samples belonged to type I, 18 samples to type II and 13 samples to type III. Staging classification was according to the

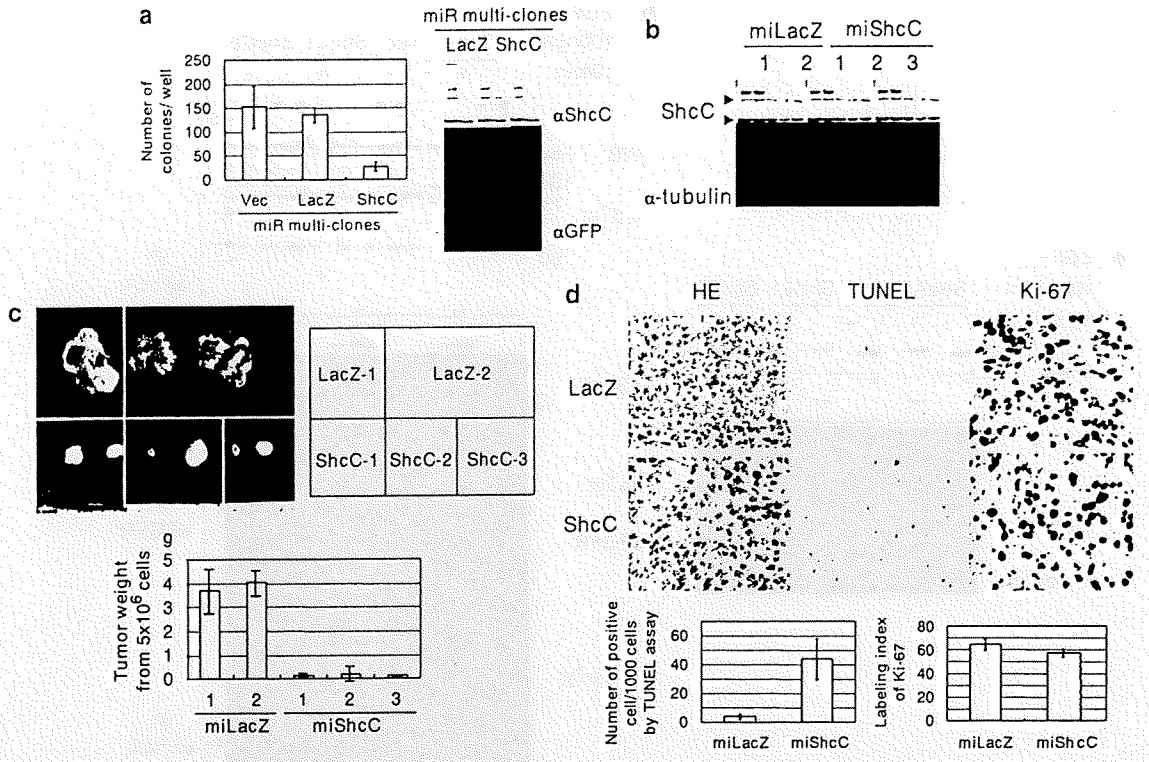

Figure 6 ShcC downregulation negatively affects tumorigenicity *in vivo*. (**a**) Cells transfected with the miR RNAi vector for ShcC (miShcC) and LacZ (miLacZ) that also contains an EmGFP coding sequence for co-cistronic expression with the pre-miRNA were cultured in medium containing blasticidin (Invivogen) for only 1 week, and then mixed. Multiclone cells for LacZ and ShcC were analysed for the ability of anchorage-independent growth using soft agar assay by 1×10^4 cells per a well of six-well plate for 3 weeks (as described in previous report: Miyake *et al*., 2005). The results represent the average value (±s.d.) of three replicated experiments. (**b**) Expression levels of ShcC in clones of TNB-1 cells stably transfected with miR RNAi expression vector for LacZ (miLacZ-1 and miLacZ-2) and ShcC (miShcC-1, -2 and -3) were detected by western analysis using αhShcC (as described in 'Materials and methods'). (**c**) Nude mouse tumors derived from two clones of LacZ miR RNAi and three clones of ShcC. Upper panel: Photographs of tumors from nude mice at 6 weeks after subcutaneous injections of 5×10^6 cloned cells (bar: 20 mm); lower panel: ability of *in vivo* tumorigenicity is shown by average weight (±) of four tumor derived from each clone. (**d**) ShcC-knockdown cells show tendency to apoptosis *in vivo*. Upper panel: Photographs of a cross-section of each tumor tissues from miLacZ-1 and miShcC-2 using microscope at a magnification of ×400, that were stained with hematoxylin and eosin (HE), diaminobenzidine (DAB) by terminal transferase dUTP nick-end labeling (TUNEL) assay and anti-Ki-67 antibody (bar: 25 μm); lower panel: the tendency to apoptosis was defined as the number of positive stained cells per 1000 tumor cells in TUNEL assay and the proliferating activity was indicated as the labeling index of Ki-67 by counting 1000 tumor cells. The data show the average scores ± s.d. of positive cells in three different areas of each slide. Staining of each sample was owing to the procedure by SRL Inc.

International Neuroblastoma Staging System and *N-Myc* amplification (> 10 copy) accepted as a poor prognostic risk factor was checked before clinical intervention.

Reagents

The polyclonal antibodies against the CH1 domain of human ShcC (amino acid 225–324):αhShcC were generated by the same method as described previously (Miyake *et al*., 2002). Polyclonal antibodies of human ShcA:αhShcA were prepared as described in previous reports (Miyake *et al*., 2002).

Other antibodies were purchased as follows: antiphosphotyrosine antibody (4G10) (Upstate Biotechnology Inc., Charlottesville, VA, USA), anti-ShcA/ShcC monoclonal antibodies: αShcA/αShcC (BD Transduction Laboratories, San Diego, CA, USA), anti-α-tubulin antibody (Zymed Laboratories, San Francisco, CA, USA), anti-p44/42 MAPK (ERK1/2), antiphospho-p44/42 MAPK (P-ERK1/2), anti-Akt, and antiphospho-Akt (Ser473) (P-Akt) antibodies (Cell Signaling, Danvers, MA, USA), anti-chromogranin A (ChrA) antibody (Santa Cruz Biotechnology, Santa Cruz, CA, USA), anti-GAP43 antibody (Zymed Laboratories), anti-MAP2 antibody (Santa Cruz Biotechnology), anti-c-Src antibody (Upstate Biotechnology Inc.), anti-phospho-Src family antibody (Tyr416) (Cell Signaling), anti-Grb2 antibody (BD Transduction Laboratories), anti-T7tag antibody (Novagen, San Diego, CA, USA) and anti-Flag M2 antibody (Sigma). As secondary antibodies, horseradish peroxidase-conjugated anti-rabbit and anti-mouse IgGs (GE Healthcare, Buckinghamshire, UK) were used. All inhibitors used in this study (PD98059, LY294002, PP2 and PP3) were purchased from Calbiochem, San Diego, CA, USA.

Cell stimulation, immunoprecipitation and immunoblotting

Cell stimulation analysis with EGF (Wako) was performed as described (Miyake *et al*., 2002). The cells were starved for 24 h and treated for 5 min with EGF (100 ng/ml). As for stimulation with collagen type I, cultured cells with or without serum for 24 h were detached from culture dishes by pipette treatment and after the suspending condition for 30 min, seeded onto a collagen type I-coated dish (Iwaki, Tokyo, Japan). Cells were harvested after 2 h using PLC lysis buffer. Control cells were harvested before the attachment on the collagen I-coated